

The first fossils of *Timon* (Squamata: Lacertinae) from Sardinia (Italy) and potential causes for its local extinction in the Pleistocene

EMANUEL TSCHOPP^{1-3,*}, ANDREA VILLA¹, MARCO CAMAITI¹, LETIZIA FERRO¹, CATERINELLA TUVERI⁴, LORENZO ROOK⁵, MARISA ARCA⁴ AND MASSIMO DELFINO^{1,6}

¹Dipartimento di Scienze della Terra, Università di Torino, Via Valperga Caluso 35, 10125 Torino, Italy

²Division of Paleontology, American Museum of Natural History, New York City, NY, USA

³Museu da Lourinhã, R. João Luís de Moura 95, 2530-158 Lourinhã, Portugal

⁴Soprintendenza Archeologia, Belle Arti e Paesaggio per le prov. di Sassari e Nuoro, Nuoro, Italy

⁵Dipartimento di Scienze della Terra, Università di Firenze, via G. La Pira 4, I-50121 Firenze, Italy

⁶Institut Català de Paleontologia Miquel Crusafont, Universitat Autònoma de Barcelona, Edifici ICTA-ICP, Carrer de les Columnes s/n, Campus de la UAB, 08193 Cerdanyola del Vallès, Barcelona, Spain

Received 21 June 2017; revised 19 December 2017; accepted for publication 23 December 2017

Timon is a large-sized lacertid lizard genus with a peculiar current distribution around the Mediterranean. Six species form three distinct clades, which are geographically separated from each other. These clades inhabit the Iberian Peninsula, France and the north-western coast of Italy (*Timon lepidus* and *T. nevadensis*); the North-African part of the western Mediterranean Basin (*T. pater* and *T. tangitanus*); and the Middle East, without connection to the Mediterranean (Turkey, Syria, Iraq and Iran; *T. kurdistanicus* and *T. princeps*). Fossil occurrences are known, but are mostly restricted to the current geographical range, with some possible exceptions from Corsica, Sicily, Malta and south-eastern Italy, none of which has yet been assessed in detail. Herein, we describe fossils from the Pleistocene of Monte Tuttavista (Sardinia, Italy), which have previously been attributed to *Lacerta* sp. Inclusion of these fossils into a phylogenetic matrix of lacertid lizards shows that they are instead referable to *Timon*. It represents the first fossil occurrence of this genus from Sardinia and confirms earlier reports of a wider distribution of the genus until the late Pleistocene. The local extinction of the genus on Sardinia seems to coincide with the appearance of predators specialized to capture small prey and with strong climatic fluctuations.

ADDITIONAL KEYWORDS: extinction – lizards – Monte Tuttavista – palaeobiogeography.

INTRODUCTION

Timon was named by Tschudi (1836) as a subgenus of *Lacerta* Linnaeus, 1758 and thus all species currently referred to *Timon* were initially proposed as species of *Lacerta*. Only in 1996, was *Timon* recognized as a distinct genus (Mayer & Bischoff, 1996), a conclusion that has since been widely accepted (Fu, Murphy & Darevsky, 1997; Harris, Arnold & Thomas, 1998; Fu, 1998, 2000; Harris & Carretero, 2003; Arnold, Arribas & Carranza, 2007; Schmidtler, 2010; Pyron, Burbrink & Wiens, 2013; Ahmadzadeh *et al.*, 2016).

Six species are currently attributed to *Timon*: *T. kurdistanicus* (Suchov, 1936), *T. lepidus* (Daudin, 1802), *T. nevadensis* (Buchholz, 1963), *T. pater* (Lataste, 1880), *T. princeps* (Blanford, 1874) and *T. tangitanus* (Boulenger, 1881) (Ahmadzadeh *et al.*, 2012, 2016; Miraldo *et al.*, 2013). Molecular and morphological phylogenetic analyses show that *Timon* is the sister-genus to *Lacerta* (e.g. Carranza, Arnold & Amat, 2004; Arnold *et al.*, 2007; Kapli *et al.*, 2011; Pyron *et al.*, 2013; Sagonas *et al.*, 2014; Mendes *et al.*, 2016), and that it includes three distinct clades, which are also geographically segregated: *T. lepidus* and *T. nevadensis* occur on the European side of the western Mediterranean basin; *T. pater* and *T. tangitanus* inhabit the North-African coast of the western Mediterranean basin; and

*Corresponding author. E-mail: etschopp@amnh.org

T. kurdistanicus and *T. princeps* are distributed in the Middle East, with no connection to the Mediterranean (Ahmadzadeh *et al.*, 2016). The divergence of the two distinct eastern and western genetic lineages of *Timon*, and the split between the European and African subclades, were estimated at 14.46 Mya and approximately 7.42 Mya, respectively, whereas the evolutionary divergence between *Lacerta* and *Timon* dates back to approximately 18.6 Mya (Ahmadzadeh *et al.*, 2016).

The vast majority of fossil remains reported in the literature were recovered from geographical areas where *Timon* still exists today (Mateo, 2009). FosFARbase lists 34 fossil occurrences referable to *Timon*, from the Gelasian to the Holocene, and from France, Spain, Portugal and Gibraltar (Böhme & Ilg, 2003). Some additional occurrences are reported by other authors, still from Quaternary localities of France and Spain (e.g. Fernández Eraso *et al.*, 2010; Bañuls Cardona *et al.*, 2012; Benítez de Lugo Enrich *et al.*, 2015). The oldest fossil might be represented by a dentary from the Pliocene of France, which constitutes the holotype of *Lacerta ruscinensis* Depéret, 1890, but was considered closely related to *Timon lepidus* by Depéret (1890) himself, Mlynarski (1956) and Estes (1983). Estes (1983) even suggested that the specimen might be referred to the extant species, resulting in *L. ruscinensis* being a junior synonym of *T. lepidus*. The absence of records from Northern Africa and the Middle East is most probably due to the very scarce knowledge of the palaeoherpetofaunas from those regions.

Reports of fossils outside the current distribution are rare, and none of them has been described or properly identified. A possible *Timon* specimen from the late Pleistocene of Germany (Brunner, 1957) was referred to *Lacerta* sp. by Estes (1983), and to *L. agilis* by Mateo (1988). Large-sized, lacertid bones from Gargano (Italy) have been referred to *Lacerta* sp. by Delfino & Bailon (2000), who also mention similarities with *Timon lepidus*. Bailon (2004) figured and described a mandible from the Middle Pleistocene of Corsica with affinities to *Timon lepidus*. Both the occurrences from Gargano and Corsica have been included in a distribution map of the genus *Timon* by Ahmadzadeh *et al.* (2016), which indicates additional fossil occurrences in Sicily (Italy) and on Malta. These fossils from Sicily and Malta most probably represent the findings of the extinct '*Lacerta siculimelitensis*' by Böhme & Zammit-Maempel (1982), although this is not explicitly stated. This enigmatic large-sized lacertid was considered to belong to *Timon* by Mateo (2009), but a detailed reassessment of the species would be needed to confirm this interpretation.

In order to improve knowledge of the insular lizards that could be related to *Timon*, herein we describe

and analyse the relationships of fossil material from the Calabrian to Upper Pleistocene fissure fillings of Monte Tuttavista (Orosei, Sardinia, Italy), which was initially referred to *Lacerta* sp. on the basis of large size (Abbazzi *et al.*, 2004), but whose morphology was not described in detail.

INSTITUTIONAL ABBREVIATIONS

The material from Monte Tuttavista was initially numbered using 'MT' as abbreviation for the locality, 'VIa' for specimens from the site 'Cava VI-antica', 'IX' for the site 'Cava IX-Prolagus' and 'BS' for the site 'Cava VIII-Blocco Strada'. This resulted in specimen numbers such as 'MT-IX-054'. All these specimens are deposited in the Soprintendenza Archeologia, Belle Arti e Paesaggio per le province di Sassari e Nuoro, Nuoro, Italy.

Other institutional abbreviations used herein are the following: CIPA, Osteoteca, Laboratorio Arqueociencias, Lisbon, Portugal; COMGR, Collezione Osteologica Mauro Grano, Roma, Italy; HUIJ-OST, Osteological Collections, Hebrew University of Jerusalem, Israel; MDHC, Massimo Delfino Herpetological Collection in the Museum of Geology and Paleontology of the Department of Earth Sciences of the University of Turin, Italy; MNCN, Museo Nacional de Ciencias Naturales, Madrid, Spain; MNHN, Muséum National d'Histoire Naturelle, Paris, France; MRAC, Musée Royal de l'Afrique Centrale, Tervuren, Belgium; NHMUK, Natural History Museum, London, UK; NHMW, Naturhistorisches Museum Wien, Vienna, Austria; PIMUZ, Paläontologisches Institut und Museum der Universität Zürich, Switzerland; SRK, Sammlung Ralf Kosma, Staatliches Naturhistorisches Museum Braunschweig, Germany; UAM, Universidad Autónoma de Madrid, Spain; ZZSiD, Institute of Systematics and Evolution of Animals, Polish Academy of Sciences, Krakow, Poland.

MATERIAL

SPECIMENS

The fossils studied herein derive from 11 fissures in quarries around Monte Tuttavista, Orosei, Sardinia. Seven of them have already been reported by Abbazzi *et al.* (2004), but new excavations in 2004 produced additional lacertid material from four more fissures in the area, as well as from the most productive fissure 'IX Prolagus', already mentioned in Abbazzi *et al.* (2004; see also Supporting Information). Abbazzi *et al.* (2004) identified two lacertid taxa in the fauna: *Podarcis* sp. and *Lacerta* sp. The same scheme was followed while cataloguing the new material from 2004,

which has thus also been tentatively referred to these two genera. Herein, we focus on the material assigned to *Lacerta* sp.

The specimens assigned to *Lacerta* include cranial, axial and appendicular elements (see [Supporting Information](#) for a detailed list). They have generally been attributed to this genus based on their large size. Some smaller bones with a similar robustness as the large elements were referred to the same taxon too, in contrast to more slender ones assigned to *Podarcis* sp. by [Abbazzi et al. \(2004\)](#).

The most complete and informative specimens were photographed with a Leica M205 C microscope. In order to avoid a limited depth of focus, image focus stacking was applied using the Leica application suite software.

GEOLOGICAL CONTEXT

The Pleistocene karst network of Monte Tuttavista is part of a massif that culminates in a small mountain range whose most prominent representative is Monte Tuttavista (806 m a.s.l.; [Abbazzi et al., 2004](#)). The substrate of Mesozoic limestone ([Dieni & Massari, 1966](#); [Dieni, Massari & Montanari, 1966](#); [Calvino et al., 1972](#)) of these mountains was subject to an intensive karst activity, resulting in a series of distinctive superficial forms such as karren, cavities, cracks and niches. The karst activity caused the creation of vertical fissures of various depths and shapes, but the prevalence of narrow fissures indicates a relatively young development of the karst. The 18 fissure-fillings of Monte Tuttavista were shown to span nearly the entire Pleistocene (just excluding the Gelasian; [Abbazzi et al., 2004](#)). Based on biochronological patterns using mostly mammals, [Palombo \(2006\)](#) tentatively dated the oldest occurrences at Monte Tuttavista to 2.2 Mya. Specimens referred to *Lacerta* sp. by [Abbazzi et al. \(2004\)](#), and subsequently by one of us (unpublished remains identified by M. Delfino), were found in fissures from all but the uppermost stratigraphic levels ([Fig. 1](#)). For a more detailed assessment of the geological context, see [Abbazzi et al. \(2004\)](#).

DESCRIPTION

The description is mainly based on the material from the fissure IX-*Prolagus*, which produced the vast majority of lacertid elements; from this fissure, 1412 bones from all parts of the skeleton were attributed to *Lacerta* sp. by [Abbazzi et al. \(2004\)](#) after subsequent excavations. There is only limited variability between the material from IX-*Prolagus* and other sites, so that only a combined description is provided here.

TERMINOLOGY

Terminology used in the description generally follows [Evans \(2008\)](#) for cranial elements, whereas for structures not named therein, we use terms by [Rauscher \(1992\)](#), [Barahona \(1996\)](#), [Daza et al., \(2008\)](#), [Klembara, Böhme & Rummel \(2010\)](#) and [Čerňanský, Smith & Klembara \(2014\)](#), indicating the sources throughout the text. For vertebral osteology, we follow [Etheridge \(1967\)](#), [Hoffstetter & Gasc \(1969\)](#) and [Tschopp \(2016\)](#); and [Lécuru \(1968, 1969\)](#) and [Russell & Bauer \(2008\)](#) are used as references for appendicular bone terminology.

CRANIAL SKELETON

Nasal

Preservation: A single, left nasal is preserved from the site IX-*Prolagus* (MT-IX-048). It lacks the tip of the anteromedial process, but is otherwise complete ([Fig. 2](#)). Its maximum anteroposterior length is 7.1 mm.

Morphology: The nasal is longer than wide. Its maximum transverse width lies somewhat more anteriorly than posteriorly. The anterior end bears the anteromedial process, which projects anteriorly from the medial margin. The posterior end is rounded. The dorsal surface bears a distinct dermal ornamentation with irregularly spaced pits of varying diameter. A deep sulcus marks the border between the prefrontal (posterior) and the frontonasal (anterior) shields; on both shields, the pits are larger towards the posteromedial corner and generally decrease in size anteriorly and laterally ([Fig. 2A](#)). This pattern is more pronounced on the ornamentation of the frontonasal shields. The sulcus between the shields extends obliquely anterolaterally to posteromedially. The ventral surface of the nasal is transversely concave in its anterior half. Within the concavity, the surface is smooth. Posterior and lateral to the concavity, where the nasal overlaps the frontal, the surface has a striated texture ([Fig. 2B](#)).

Frontal

Preservation: None of the frontals is complete: the anterior frontal–nasal margin is damaged in all elements, and often completely missing, as are the lateral and medial processes ([Fig. 3](#)). The longest and most complete frontal, MT-IX-012 ([Fig. 3A, B](#)), is 15.4 mm long. Additional measurements are provided in the [Supporting Information](#).

Morphology: The vast majority of the frontals are large and unpaired, and are composed of two fused symmetrical elements. The longitudinal suture line is not clearly recognizable in the posterior portion of the ventral surface, but a remnant of it is visible anteriorly

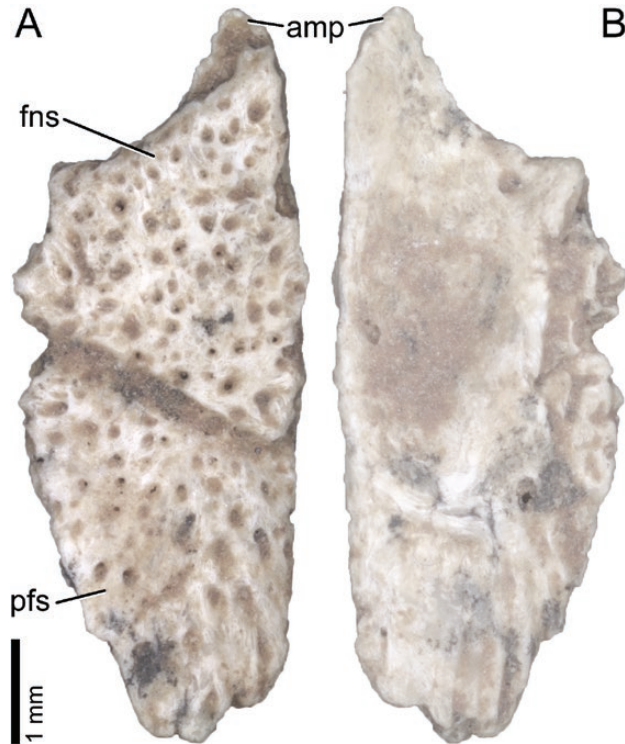


Figure 2. Left nasal of *Timon* sp. (MT-IX-048) in dorsal (A) and ventral (B) views. Abb.: amp, anteromedial process; fns, frontonasal shield; pfs, prefrontal shield.

anteriorly, and a smaller one for the postfrontal posteriorly (Fig. 3B, D). They are very far from each other. Ventrally, the most complete specimens bear two long and distinct anterior processes on the anterior half, which originate from the cranial crests. These crests are parallel, and extend throughout the entire length of the frontals, along the lateral margins (Fig. 3B, D).

Variability: Not all frontals are fused. A few single frontals exist among the specimens from Monte Tuttavista. There is some variability in the shape of the impression of the prefrontal shield. In some specimens, the sulci delimiting the prefrontal shields posteromedially meet each other at the midline (Fig. 3C), whereas in the majority of specimens they

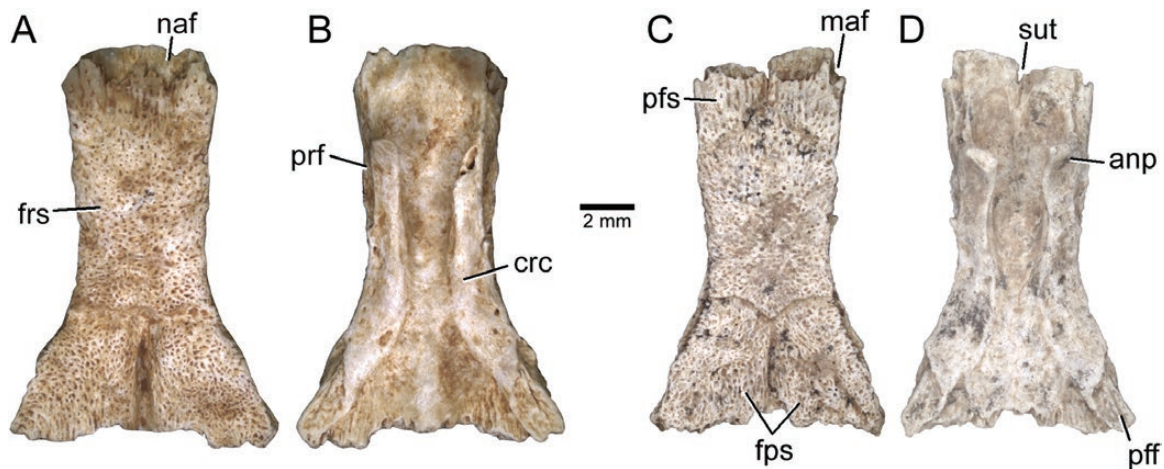


Figure 3. Frontals MT-IX-012 (A and B) and MT-IX-049 (C and D) of *Timon* sp. in dorsal (A and C) and ventral (B and D) views. Abb.: anf, anterior process; crc, cranial crest; fps, frontoparietal shield; frs, frontal shield; maf, maxillary facet; naf, nasal facet; pff, postfrontal facet; pfs, prefrontal shield; prf, prefrontal facet; sut, suture.

remain separated throughout their length. Two small, fused frontals, which bear the distinct anterior sulci, have more concave lateral margins compared to the larger elements, which probably represent ontogenetic changes (Barahona & Barbadillo, 1998).

Parietal

Preservation: Most of the large parietals are moderately well-preserved. Some elements lack their anterior part, and in all but one parietal, the parietal tabs are broken off. The postparietal processes are also rarely preserved. The largest preserved parietal (MT-IX-009; Fig. 4A, B), has a length of 13.7 mm and a maximum width of 11.1 mm (across the dorsal, ornamented part). Additional measurements are provided in the Supporting Information.

Morphology: The parietals have a longer than wide parietal shelf, which is completely covered by a well-developed dermal ornamentation. The anterior margin is relatively straight, with a slight interdigitation, such as in MT-IX-010 (Fig. 4C, D), but this could be due to taphonomic reasons. The lateral margins are almost straight and subparallel, creating a subrectangular facies parietalis. The posterior margin is nearly straight. The dorsal ornamentation shows six distinct, symmetrically placed shields separated by grooves: two bilaterally symmetrical frontoparietal shields anteriorly, the interparietal shield in central position, two lateral shields (*sensu* Klembara *et al.*, 2010) posterolaterally and the occipital shield posteromedially. A subelliptical parietal foramen pierces the shelf in the middle of the interparietal shield. The occipital shield is of approximately the same anteroposterior length as the interparietal shield and of similar, to slightly larger, transverse width. It is not considerably expanded mediolaterally at its posterior margin, unlike the condition in *Timon lepidus* (Arnold *et al.*, 2007), occupying about a third to a half of the entire posterior width of the ornamented dorsal surface of the parietal. The postparietal processes are robust and distinctly widened proximally. These processes project posterolaterally and appear to curve slightly laterally in the most complete specimens (e.g. MT-IX-010; Fig. 4C, D). Well-developed ventral crests are visible on the ventral surface. The anterolateral ventral crests form a V-shape, converging posteriorly in a narrow, longitudinal ridge, which extends along the midline between the facies triangularis (*sensu* Rauscher, 1992) and the parietal fossa (Fig. 4B, D). They do not meet the proximal end of the posterolateral ventral crests. The parietal fossa is deep and tapers anteriorly to a point. There is no parietal notch, nor a projection along the posterior margin.

Variability: There is some variation in the posterior width of the occipital shield relative to the posterior margin of the ornamented surface. In particular, a

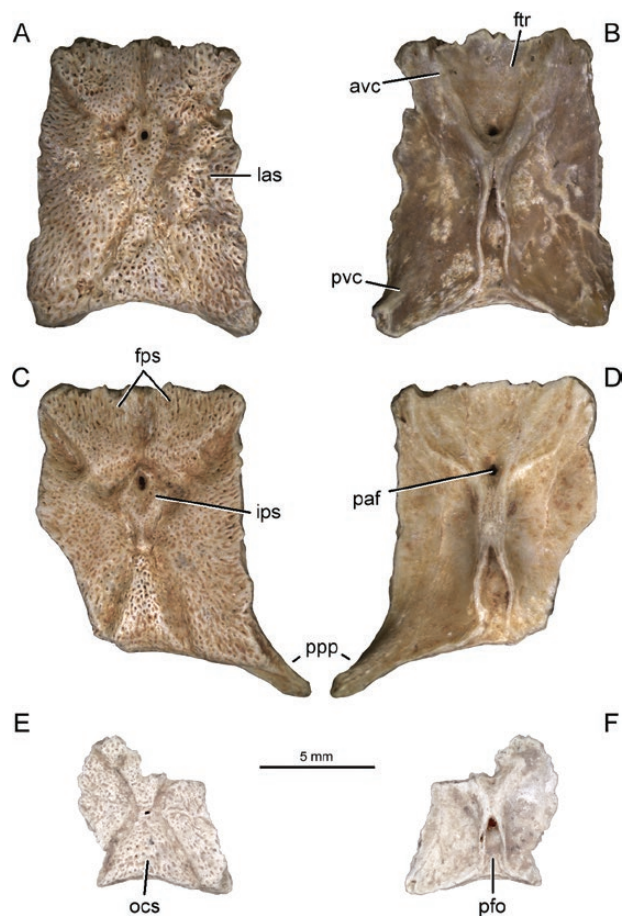


Figure 4. Parietals MT-IX-009 (A, B), MT-IX-010 (C, D), and MT-IX-050 (E, F) of *Timon* sp. In dorsal (A, C, E) and ventral (B, D, F) views. Note the differing relative lengths and widths of the occipital shield. Abb.: avc, anterolateral ventral crest; fps, frontoparietal shield; fr, facies triangularis; ips, interparietal shield; las, lateral shield; ocs, occipital shield; paf, parietal foramen; pfo, parietal fossa; pvc, posterolateral ventral crest; ppp, postparietal process.

small parietal (MT-IX-050; Fig. 4E, F) has a relatively much wider occipital shield than larger specimens, but this could also be due to ontogeny, as occurs in *Gallotia* (Barahona & Barbadillo, 1998). There is also some variation in the length of the interparietal and occipital shields (see Supporting Information). However, all the parietals where measurements of these two shields could be taken, have a proportionally much longer occipital shield than most of the specimens of *Lacerta* studied herein.

Premaxilla

Preservation: The premaxillae are variably complete (Fig. 5). Many of them lack at least part of the ascending nasal process, and some preserve only one-half of the tooth-bearing portion. The maximum width

of the tooth-bearing portion reaches up to 5.52 mm (estimated from the left-half).

Morphology: The premaxillae are large and bear a leaf-shaped ascending nasal process. The nasal process projects straight posterodorsally, and is slightly dorsoventrally constricted at about midlength. It forms an acute angle with the horizontal plate in lateral view. A pair of ethmoidal foramina (*sensu* Klembara *et al.*, 2010) for the longitudinal canals is visible at the base of the process (Fig. 5A). The anterodorsal surface of the process is covered by a well-developed dermal ornamentation in its dorsal half. The lateral margins are smooth and slightly concave in the anteroventral portion, and expand transversely up to the ventral-most extension of the ornamentation. From there, the margins taper irregularly towards their pointed posterodorsal end. The posteroventral surface of the ascending nasal process is marked by a distinct medial

ridge, which extends longitudinally along the midline of the process, and is flanked posterolaterally by distinct articular facets for the nasals (Fig. 5B, E). The ridge is only distinct in the dorsal part and appears to fade gradually towards the tip in one element (MT-IX-002; Fig. 5F), whereas in the elements with a preserved dorsal tip, the medial ridge forms a distinct posterodorsal process below the tip of the dorsal shelf of the nasal process (see MT-IX-001; Fig. 5C). The contact between the ascending nasal process and the tooth-bearing portion is slender, with an ellipsoid to subtriangular, anteroposteriorly compressed cross-section. The tooth-bearing portion is robust and consists of an anterior, vertical alveolar plate and a posterior, horizontal plate (*sensu* Rauscher, 1992), which bears two posteriorly projecting palatine processes. In dorsal view, the alveolar plate and the lateral margin of the horizontal plate form approximately a right angle. Except for the fragmentary elements, the premaxillae

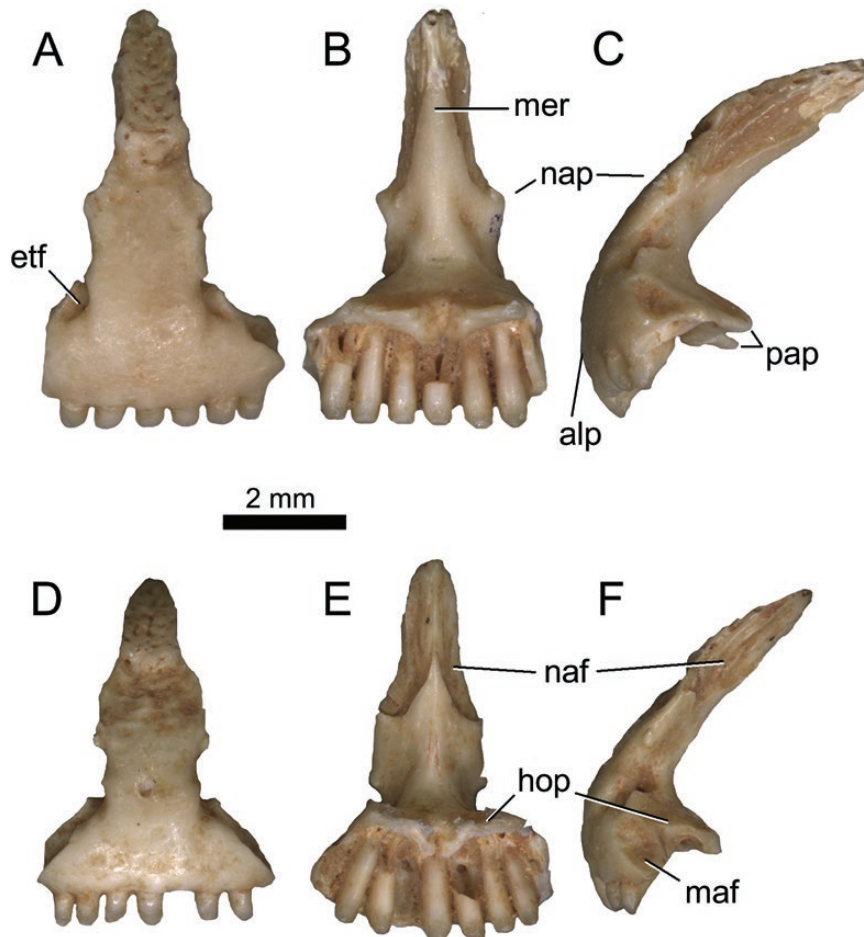


Figure 5. Premaxillae MT-IX-001 (A–C) and MT-IX-002 (D–F) of *Timon* sp. in anterior (A, D), posterior (B, E), and left lateral (C, F) views. Note the different morphology of the dorsal end of the medial ridge in lateral view (C, F). Abb.: alp, alveolar plate; etf, ethmoidal foramen; hop, horizontal plate; maf, maxillary facet; mer, medial ridge; naf, nasal facet; nap, ascending nasal process; pap, palatine process.

have eight or nine pleurodont, cylindrical and moderately slender teeth. In the elements without a complete tooth-bearing portion, the estimated tooth count is always eight or more. The crowns are too worn to clearly state whether all teeth were unicuspid or if bicuspid ones were also present. The teeth are smaller than the maxillary teeth. The palatine processes are usually broken posteriorly, but in the best-preserved specimens, a wide, V-shaped notch seems to separate them.

Variability: There is a certain degree of individual variation in the development of the ornamentation. Also, the two foramina are enclosed to varying degrees. Generally, they are bordered by a bony ridge posteriorly and accompanied anteriorly by a subtriangular, laterally projecting process on the anterolateral margin of the ascending nasal process. In some premaxillae, the foramina are anteriorly bordered by an additional crest connecting the nasal process with the alveolar plate. Where it occurs, this anterior crest is pierced by a second foramen for the longitudinal canals. An additional, smaller foramen sometimes pierces the posterior surface of the ascending nasal process ventrally. An apparent variation in the shape of the dorsal end of the medial ridge is often due to breakage of the tip of the ascending nasal process. However, most elements have a bifid posterodorsal end of the nasal process when seen in lateral view.

Maxilla

Preservation: The preservational status of the maxillae varies from very well-preserved to fragmentary. The dorsal, prefrontal processes (*sensu* Rauscher, 1992) are often lacking. The largest elements reach anteroposterior lengths greater than 15.5 mm.

Morphology: The maxillae are large, robust and bear a subtriangular facial process (Fig. 6). The anterior premaxillary process is bifurcated, with well-developed anterolateral and anteromedial processes, defining a deep and U- to V-shaped anterior concavity (Fig. 6A). A distinct and robust lappet is present on the dorsal surface of the anteromedial process. The concave area housing the vomeronasal foramen is shallow; it is marked laterally by a very low ridge, whereas medially there is a more developed and robust ridge, which merges with the lappet. The lateral surface of the facial process is covered by a well-developed dermal ornamentation on its dorsal portion, which can display deep sulci marking the contact of the different scales. Ventrally to the ornamented area, the lateral surface bears five to seven labial foramina. The facial process bears two prefrontal processes dorsally, which (when preserved) are weakly developed, and form two short and wide posterodorsal projections (Fig. 6A, C).

The medial surface of the facial process is marked by a low, arched ridge. The superior alveolar foramen is very wide and opens in the posterior direction into a wide groove. The posterior process is wide and tapers posteriorly; in dorsal view, it tends to curve in a lateral direction towards the posterior end (Fig. 6A). In lateral view, the dorsal margin of the posterior process is not stepped, unlike the condition seen in *Lacerta* (Arnold *et al.*, 2007). The tooth row follows the lateral curvature or the posterior end to some degree (Fig. 6D). The maxillary teeth are very robust and clearly hypertrophied in the central part of the tooth row, decreasing in size towards the anterior and posterior extremities. They are pleurodont, cylindrical and strongly worn. In some specimens, however, it is possible to recognize a mono- and a bicuspid condition. The tooth row ends very close to the posterior end of the bone and carries 11 to 15 teeth in the best-preserved specimens.

Variability: There appears to be some variability in the curvature of the maxillary shelf and in the length of the prefrontal processes, but these differences are mostly due to the fact that the dorsal-most portion of the maxillae is almost always broken. A clear difference can be seen in a single left maxilla, which has a weak, bulbous bony outgrowth on the lateral surface, of probably pathological origin. There is also variability in the tooth development, with some elements bearing strongly enlarged teeth in the posterior, and sometimes also the anterior, half of the tooth row.

Jugal

Preservation: The jugals are generally well-preserved. Only the tips of the branches of the bone are usually broken off. The largest jugal from IX-*Prolagus* measures 14.4 mm in a straight distance from the posterior-most point of the quadratojugal process to the anterior-most point of the anterior process.

Morphology: The jugals are L-shaped in lateral view, with an anterior and a posterodorsal process (Fig. 7). All specimens show a well-developed anterior process, whose anterior part bears a large facet for the articulation with the maxilla on the lateral surface, and was, therefore, scarcely exposed in the articulated skull (Fig. 7A). The rest of the lateral surface of the anterior process is covered by a well-developed dermal ornamentation. Along the medial surface of the maxillary process, a palatal process projects weakly medially, forming the anterior portion of the medial ridge (*sensu* Čerňanský *et al.*, 2014). The posterior end of the palatal process bears a short, but clearly distinct, medial process (Fig. 7B). From there, the medial ridge extends posterodorsally along the anterior edge of the posterodorsal process, and a

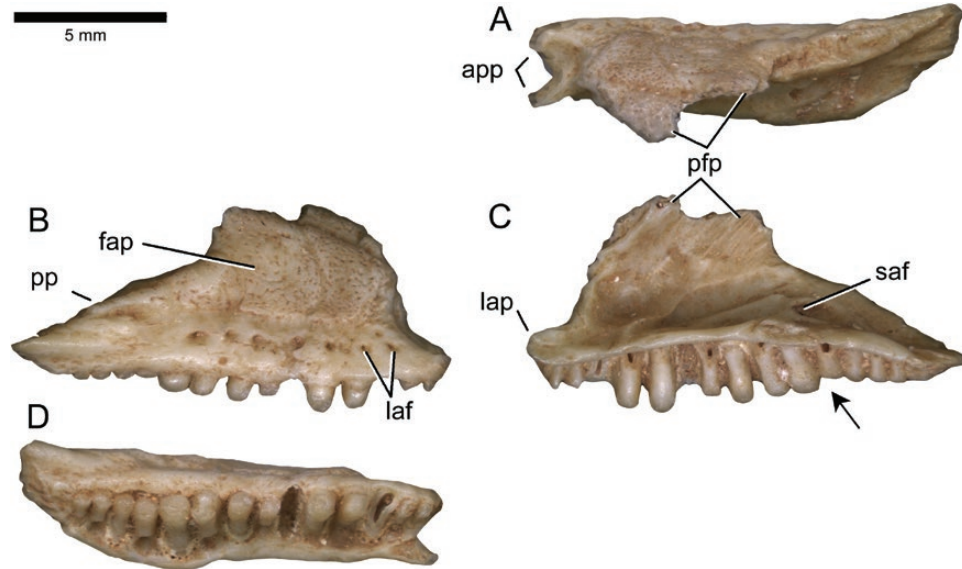


Figure 6. Right maxilla of *Timon* sp. (MT-IX-006) in dorsal (A), lateral (B), medial (C), and ventral (D), views. Note the abrupt change from enlarged to small teeth in the posterior part of the tooth row (arrow in C). Abb.: app, anterior premaxillary process; fap, facial process; laf, labial foramen; lap, lappet; pfp, prefrontal process; pp, posterior process; saf, superior alveolar foramen.

third, short crest extends posteroventrally. The distal end of the posterodorsal process is often lacking, but where it is preserved, it curves distinctly posteriorly towards its tip. On its medial surface, a very distinct and large articular surface with the postorbital marks the dorsal end. A small, interior zygomatic foramen pierces the medial process posteriorly. The quadratojugal process is large and distinct (Fig. 7C, D), and emerges from the bony shelf that expands from the posterodorsal process.

Variability: The sample of jugals does not show any variability in morphology.

Postfrontal–postorbital

Preservation: Only one of these bones is reasonably complete, but all of them lack variable portions of their posterior section. The tips of the anterior processes are often broken as well. The most complete postfrontal–postorbital has an anteroposterior length of 13.6 mm.

Morphology: The postfrontals and postorbitals are always fused (Fig. 8). Because the posterior-most end is always broken, it is unclear which of the two components was longer and if the postorbital formed a pointed posterior process, as sometimes occurs in *Lacerta schreiberi*. The anteromedial (frontal) process is longer than the anterolateral (jugal) process, and the two form an angle of approximately 70°. Between the two, there is a short, anterior subtriangular projection (Fig. 8A). A similar projection marks the extension of the supraocular osteoderms in

Psammodromus algirus NHMW 788, but is absent in *Lacerta viridis* (Rauscher, 1992: abb. 5; Fig. 3A) and in *Timon lepidus* MDHC 216. From a point straight ventral to this projection, a weak ridge extends towards the medial edge, almost perpendicular to the long axis of the bone, and crossing the anteromedial process ventrally. The articular facets for the frontal and the jugal are on the medial and lateral surfaces of the respective processes. The frontal facet is more deeply concave than the jugal facet. The latter is also marked by a longitudinal, weak ridge, dividing the concavity into a dorsal and a ventral portion. The dorsal surface is nearly entirely covered by dermal ornamentation. Only the anteromedial portion and the anteromedial process lack such a cover. The ornamentation is marked anterolaterally by an oblique sulcus, which marks the border between the lateral, parietal shield medially and the most anterior supratemporal one laterally. This sulcus is located more medially in *Timon lepidus* MDHC 216, and extends further posteriorly than in the material from Monte Tuttavista. The lateral position of this sulcus in the fossil material is similar to the condition in some individuals of the genera *Algyroides*, *Archaeolacerta*, *Phoenicolacerta*, *Podarcis*, *Scelarcis* and *Teira* (Arnold *et al.*, 2007). The entire dorsal surface is strongly convex transversely. The ventral surface is concave. This concavity is distinctly bordered anteriorly and anteromedially. The medial margin is always damaged anteriorly, so that it is impossible to tell whether it was expanded or not.

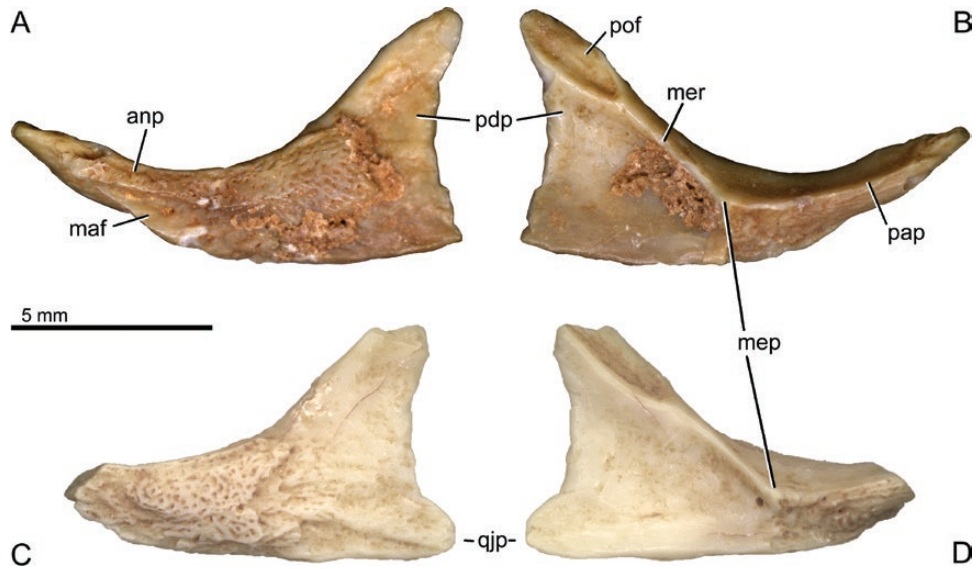


Figure 7. Left jugals MT-IX-015 (A, B) and MT-IX-097 (C, D) of *Timon* sp. in lateral (A, C) and medial (B, D) views. The quadratojugal process of MT-IX-015 and the anterior process of MT-IX-097 are incomplete. Abb.: anp, anterior process; maf, maxillary facet; mep, medial process; mer, medial ridge; pap, palatine process; pdp, posterodorsal process; pof, postorbital facet; qjp, quadratojugal process.

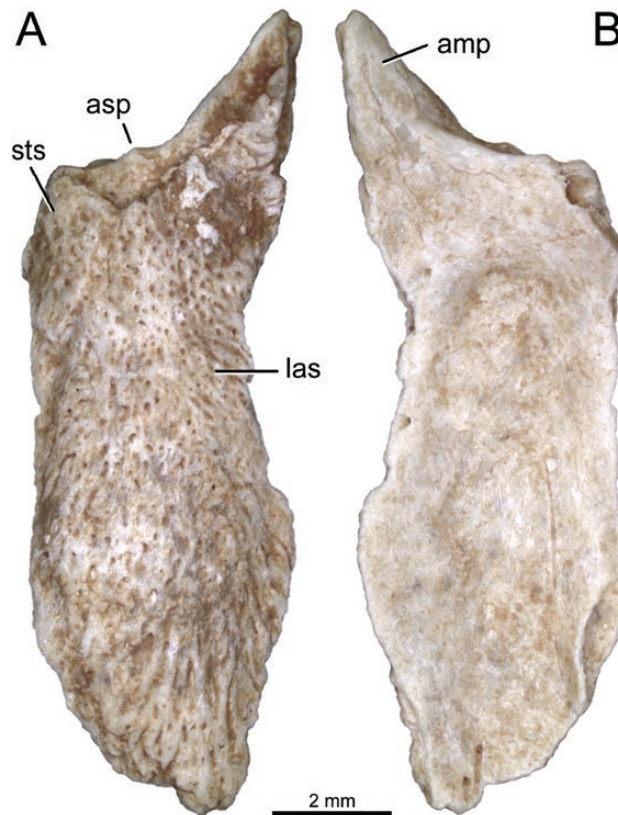


Figure 8. Left postfrontal–postorbital of *Timon* sp. (MT-IX-069) in dorsal (A) and ventral (B) views. Abb.: amp, anteromedial process; asp, anterior subtriangular projection; las, lateral shield; sts, supratemporal shield.

Variability: There is some minor variability in the size of the short, subtriangular, anterior projection, and in the depth of the sulcus separating the parietal and supratemporal shields.

Quadrates

Preservation: The quadrates are generally well-preserved and complete. A small number of elements lack parts of their medial edge. The largest element has a dorsoventral length of 7.4 mm and a maximum transverse width of 5.4 mm.

Morphology: The quadrates from Monte Tuttavista are very stout elements (Fig. 9). The cephalic condyle has a subrectangular outline, being slightly longer than wide. A small tubercle marks its medial margin, from where a short ridge extends ventrally to ventromedially on the medial surface of the central pillar (Fig. 9B). The anterior surface of the quadrate has a complex morphology. It is generally concave transversely and convex dorsoventrally. Dorsally, it bears a very distinct, slightly concave anterior platform on the lateral half. The anterior platform forms a distinct, pointed ventral step and is strongly offset from the rest of the anterior surface. Because of this pointed ventral step, the anterior margin of the quadrate has an angular shape in medial and lateral view (Fig. 9B). The medial edge of the anterior surface is strongly transversely expanded close to the cephalic condyle, and tapers to a crest in the ventral half. It bears a distinct, medially projecting pterygoid process close to its ventral end, which articulates with the pterygoid. This pterygoid process is regularly rounded and has a semi-circular outline in anterior view. The posterior surface of the quadrate is marked by the central pillar, which is situated on the medial half of the bone. The mandibular condyle is saddle-shaped, being concave transversely and convex anteroposteriorly. The two

elevated hemicondyles are angled with respect to the transverse axis of the articular surface. The lateral one is slightly larger than the medial one. The tympanic crest is very robust, showing a distinct enlargement at midheight. It marks the lateral margin of a deep conch.

Variability: In some elements, the anterior surface is pierced by a small foramen, right above the mandibular condyle (Fig. 9A).

Braincase

Preservation: Three braincases (otoccipital regions) were preserved in the Cava VI-antica. They all lack the tips of the supraoccipital, of the paroccipital processes and most of the basisphenoid. The largest element (MT-VIa-001; Fig. 10) has a foramen magnum with a maximum diameter of 3.3 mm.

Morphology: The otoccipital regions are very large and robust. The different bones composing the region are completely fused in all three specimens. Overall, the region is not dorsoventrally compressed. The foramen magnum is large and circular. The paroccipital processes, although lacking their distal extremities, are long, indicating a transversely wide posterior end of the skull. On the lateral surface, anteroventral to the paroccipital process, the lateral opening of the recessus scalae tympani is very wide and anteroposteriorly elongate (Fig. 10C). The fenestra ovalis is situated dorsal to the lateral opening of the recessus and is only slightly smaller than the latter (Fig. 10C). The recessus scalae tympani is furthermore pierced by the medial opening of the recessus and the perilymphatic foramen, which are wide and subelliptical. The semi-circular canals are poorly visible externally. The occipital condyle is robust and shows no posterior notch in ventral view (Fig. 10A). Given the complete

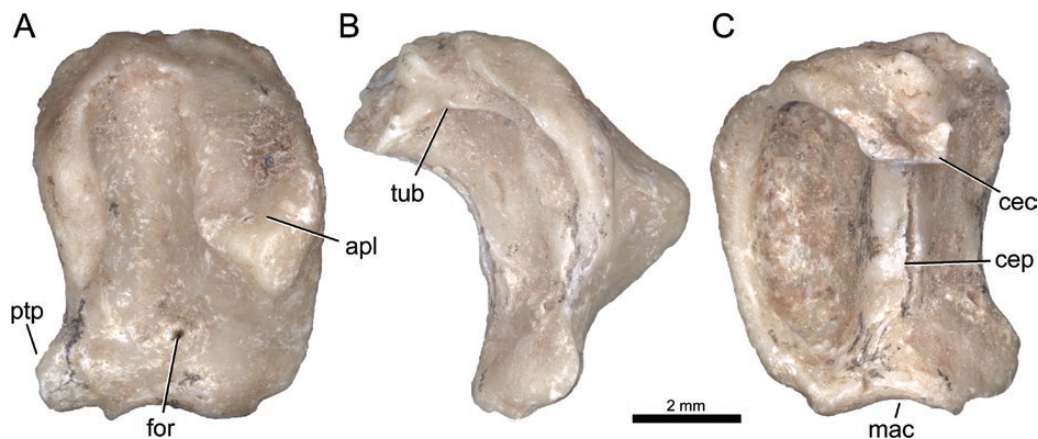


Figure 9. Left quadrate of *Timon* sp. (MT-IX-054) in anterior (A), medial (B), and posterior (C) views. Abb.: apl, anterior platform; cec, cephalic condyle; cep, central pillar; for, foramen; mac, mandibular condyle; ptp, pterygoid process; tub, tubercle.

fusion of the bones composing the braincase, it is not possible to recognize the different components of the condyle (basioccipital and otoccipital). The basioccipital is mushroom-shaped and wider than it is long in ventral view, with the posterolateral sides being composed of ridge-like expansions. The sphenoccipital tubercles on the basioccipital are well developed. Both the ventral and the dorsal surface of the basioccipital are smooth. The sphenoid is generally lacking, but incompletely preserved in a single specimen (MT-VIa-002), in which it preserves part of the posterior half, which is marked by a strong, anteroposteriorly extending concavity. The supraoccipital bears a very robust, cylindrical and well-developed processus ascendens, which is broken in all specimens. The posterodorsal surface of the processus is marked by a sharp and well-developed supraoccipital crest extending vertically along the midline (Fig. 10D). In dorsal view, the anterolateral margins of the bone are convergent. The prootics always lack most of both the alar and the anterior inferior processes. The posterior process of the prootic is long and a well-developed (but generally broken) crista prootica extends along the posterior projection (Fig. 10C). Ventrally to the crista, and anterior to

the fenestra ovalis, there is a moderately large facial foramen, whose anterior margin is marked by a high ridge that partially covers the foramen in lateral view. The prootic portion of the recessus vena jugularis (*sensu* Daza *et al.*, 2008), which is very shallow and clearly recognizable only in MT-VIa-002 because of the preservation of the posterior openings of the vidian canals, ends ventral to the facial foramen. The otoccipital bears very long and robust paroccipital processes, whose distal ends are never preserved. The vagus foramen is moderately small compared to the hypoglossal foramina (Fig. 10C). Three hypoglossal foramina are recognizable in the specimen in which this area is best preserved (MT-VIa-002).

Variability: There is no significant variation in the three braincases from Cava VI-antica.

Pterygoid

Preservation: All the pterygoids are moderately preserved. Most elements lack the tips of the palatine process and the pterygoid flange. The quadrate process is moderately preserved in MT-IX-014 and MT-IX-027, and mostly lacking in MT-IX-013. One of the largest specimens (MT-IX-014) has a preserved anteroposterior length of 14.4 mm.

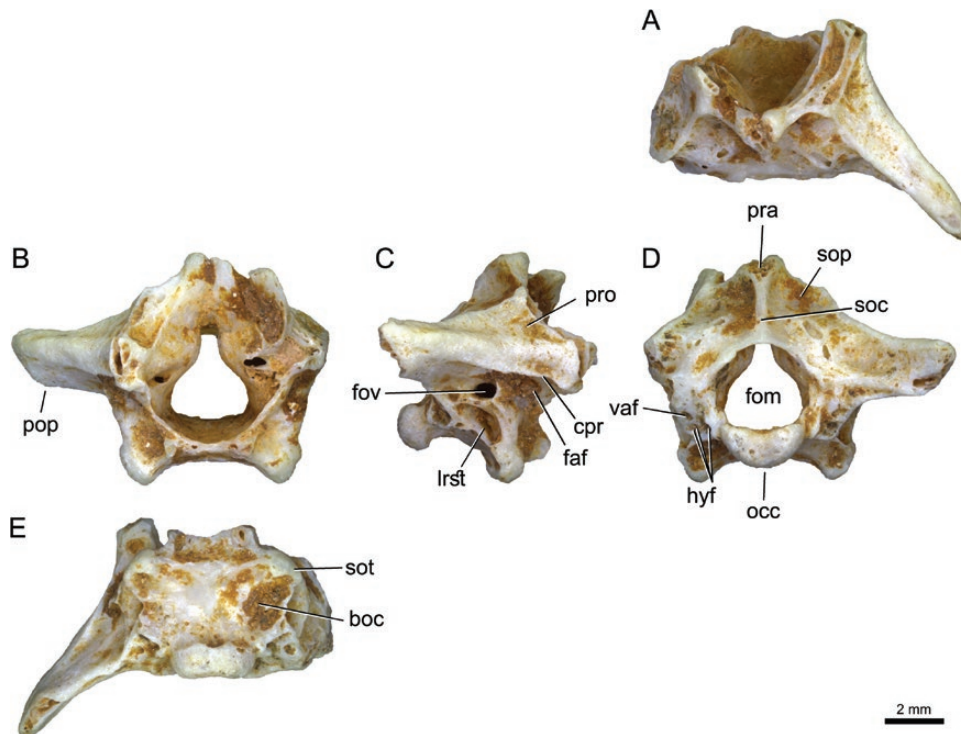


Figure 10. Braincase MT-VIa-001 of *Timon* sp. in dorsal (A), anterior (B), right lateral (C), posterior (D), and ventral (E) views. The facial foramen is covered by matrix. Abb.: boc, basioccipital; cpr, crista prootica; faf, facial foramen; fom, foramen magnum; fov, fenestra ovalis; hyf, hypoglossal foramen; lrst, lateral opening of recessus scalae tympani; occ, occipital condyle; pop, paroccipital process; pra, processus ascendens; pro, prootic; soc, supraoccipital crest; sop, supraoccipital; sot, sphenoccipital tubercles; vaf, vagus foramen.

Morphology: The general shape of the pterygoids is triradiate, with an anteromedial palatine process, an anterolateral pterygoid flange and a posterolateral quadrate process (Fig. 11). The palatine process is a large and laminar structure, provided with a low number of cylindrical, moncuspid pterygoid teeth (three on average; Fig. 11A). Despite the breakage, the pterygoid flange displays well-developed dorsal and ventral ridges. Because of the preservational status of the anterior end, it is not possible to clearly recognize the complete development of the concave pterygoid recess. However, comparisons with complete extant material of *Lacerta* and *Timon* indicate that the recess is rather weakly developed, approaching an angle of about 90° between the palatine process and the pterygoid flange. The quadrate process is large, extended posteriorly and mediolaterally compressed. It shows a deep and subelliptical fossa columellae, which is the articular surface for the epipterygoid, and a strongly developed pterygoid ridge. The pterygoid ridge extends posterior to the columellar fossa, along the dorsolateral margin of the quadrate process. On the medial surface, a shallow basiptyergoid fossa continues posteriorly in a wide and strongly concave surface, forming the facet for the articulation with the basiptyergoid process of the sphenoid. The pterygoid groove is located on the ventromedial surface of the quadrate process, where the pterygoid meniscus inserts (Fig. 11A).

Variability: In most elements, the teeth are anteroposteriorly aligned to form a kind of tooth row, whereas in some pterygoids, they are aggregated, forming a small patch (e.g. MT-IX-014; Fig. 11A). None of the preserved pterygoids shows a V-shaped pattern, as has been described in some species of *Gallotia* (Barahona *et al.*, 2000). In the latter genus, a change in the tooth arrangement can occur during ontogeny, but can also be taxonomically important (Barahona *et al.*, 2000). Among the specimens from Monte Tuttavista, elements of comparable size can bear both patches and tooth rows, arguing against ontogenetic differences in tooth arrangement in this case. However, the same is the case in specimens of *Timon lepidus* (e.g. NHMW 699 has a patch, whereas MRAC 3390 has a tooth row), showing that this feature can be individually variable in certain large-sized lacertid genera. The quadrate process and the pterygoid flange form angles between approximately 110° and 90°. The dorsal surface of the bony shelf between the palatine process and the pterygoid flange sometimes bears a distinct crest delimiting the articular facet for the ectopterygoid medially. The ventral transverse crest is often distinct, but is weakly expressed in some elements.

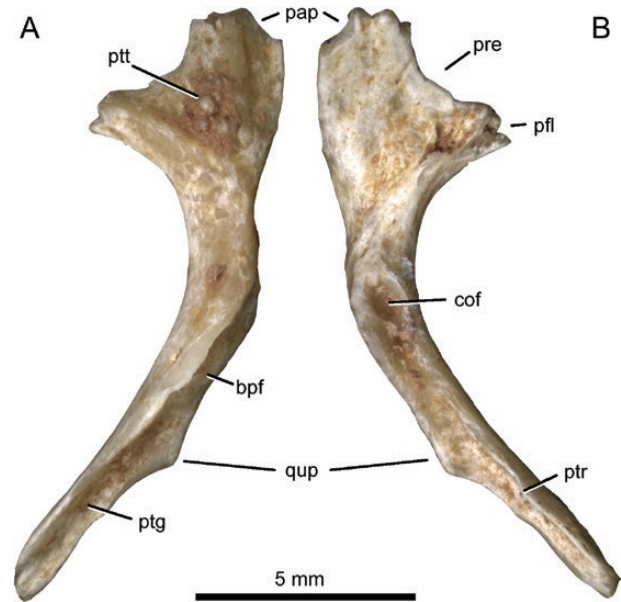


Figure 11. Right pterygoid of *Timon* sp. (MT-IX-014) in ventral (A) and dorsal (B) views. Abb.: bpf, basiptyergoid fossa; cof, columellar fossa; pap, palatine process; pfl, pterygoid flange; pre, pterygoid recess; ptg, pterygoid groove; ptr, pterygoid ridge; ptt, pterygoid teeth; qup, quadrate process.

Ectopterygoid

Preservation: The only preserved ectopterygoid (MT-IX-068; Fig. 12) lacks the tips of its three processes. The preserved anteroposterior length of the lateral articular facet for the external skull is 5.6 mm.

Morphology: The ectopterygoid is a triradiate element and connects the pterygoid with the maxilla. It has a long, tapering anterolateral process. A posterolateral process was present, as indicated by a broken bone surface, but it is impossible to tell if it was well developed, as in *Takydromus* (Gauthier *et al.*, 2012), or not. The posteromedial process expands dorsoventrally towards its medial end, where it is bifurcated, and clasps the pterygoid flange (*sensu* Evans, 2008) of the pterygoid dorsally, anteriorly and ventrally. Due to the incomplete preservation, it is impossible to tell which of the lappets is the longest.

Dentary

Preservation: The preservational status of the dentaries varies between fragmentary and moderately well-preserved. Only few remains show both the coronoid and the angular processes. Furthermore, the surangular process is almost always lacking. The dentaries reach preserved lengths greater than 18.3 mm.

Morphology: The dentaries are generally large and robust (Fig. 13), but smaller specimens are also

present. The mandibular symphysis is narrow, but distinct, and slightly dorsally inclined in medial view. The lateral surface of the dentary is convex dorsoventrally and pierced by a variable number of anteroposteriorly aligned mental foramina (Fig. 13A, C). Posterodorsally, it bears a distinct articular surface for the coronoid (Fig. 13C). The Meckelian fossa opens medially along the entire length of the dentary, being narrow anteriorly and gradually widening posteriorly. The subdental ridge is robust, slightly dorsoventrally expanded anteriorly but narrowing posteriorly. When preserved, the ventral angular process is posteriorly directed and pointed. The dorsal coronoid process, on the other hand, is always damaged and, therefore, its size and shape are never recognizable. The teeth are pleurodont and cylindrical; always more than 13, up to a maximum of 17. A substantial portion of their crowns is covered laterally by the dental crest, such that less than half of the crown is visible in lateral view. The largest teeth are located in the distal half of the tooth row, but do not occupy the distal-most positions. In some dentaries, the distal three to seven teeth are considerably smaller than the preceding ones (Fig. 13B). Anterior teeth seem to be monocuspid, but it is usually difficult to recognize the crown morphology of the other teeth because of strong tooth wear. Nevertheless, a distinct bicuspid or even tricuspid condition in the central teeth is clearly visible in some specimens.

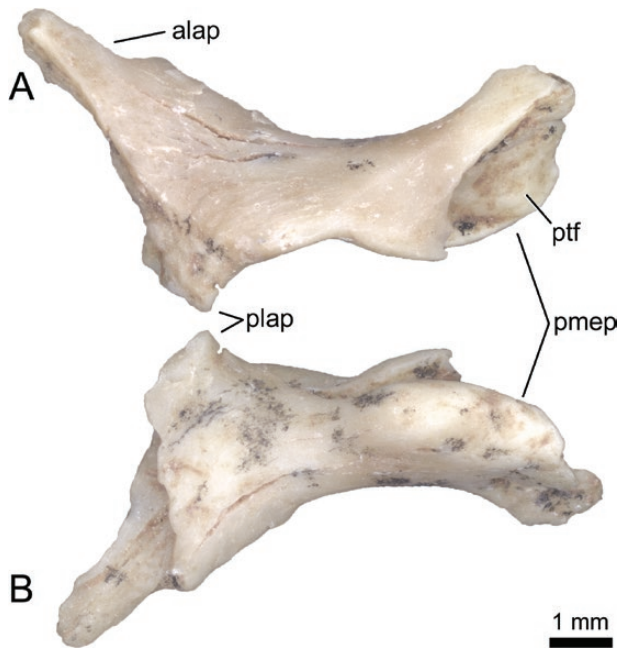


Figure 12. Left ectopterygoid of *Timon* sp. (MT-IX-068) in dorsal (A) and ventral (B) views. Abb.: alap, anterolateral process; plap, posterolateral process; pmep, posteromedial process; ptf, pterygoid facet.

Variability: The variation in the dentaries is the most significant. The lateral surface of the dentary can either be smooth (in most cases) or marked by a more or less distinct cover of dermal ornamentation (Fig. 13C). Similarly sized specimens can either present the ornamentation or not. Some specimens show a rather gradual decrease in tooth size posteriorly, whereas others show an abrupt transition from large to small teeth. The number of small distal teeth is variable as well, reaching up to seven teeth in some dentaries. An abrupt transition, and such a high number of small distal teeth (Fig. 13B), have initially been proposed as diagnostic features of the extinct lacertid '*Lacerta*' *siculimelitensis* (Böhme & Zammit-Maempel, 1982; see also Delfino, 2001). However, this species has later generally been considered invalid, mostly because the variability in the dentition of *Timon* appears also to include such extreme cases as has been considered autapomorphic for '*L.*' *siculimelitensis* (Mateo, 1988). The dorsal projection of the coronoid process is variable in the sample from Monte Tuttavista, sometimes even involving the distal teeth (Fig. 13A), similar to the Miocene taxa *Ligerosaurus* (Augé, Bailon & Malfay, 2003) and *Janosikia* (Čerňanský, Klembara & Smith, 2016). In other specimens, the process does not extend considerably dorsal to the tooth row.

Splénial

Preservation: A single, left splénial is preserved, articulated with the dentary (Fig. 13C, D). It is complete, and has a length of 15.9 mm.

Morphology: The splénial is a transversely thin and flat bone, which covers most of the Meckelian fossa medially. Anteriorly, it reaches nearly to the symphysis. It has a rhomboid outline in medial view, with pointed anterior and posterior ends. The tallest dorsoventral height is located below the distal-most teeth. A large, anterior inferior alveolar foramen pierces the splénial at around midlength, and a second, small, mylohyoid foramen occurs right-ventral to the large one, separated from it by a very narrow, horizontal bony bridge. The medial surface of the splénial is weakly concave dorsoventrally.

Coronoid

Preservation: The three coronoids from the site IX-*Prolagus* are all of different sizes, and lack the tips of their anterolateral, anteromedial and posteromedial processes. The largest element (Fig. 14) has a preserved dorsoventral height of 7.2 mm.

Morphology: The coronoids have an inverted V-shape in lateral view. There are two anterior processes (the anteromedial and labial processes), a posterior one (the posteromedial process) and a dorsally projecting coronoid process. The angle between the anteromedial

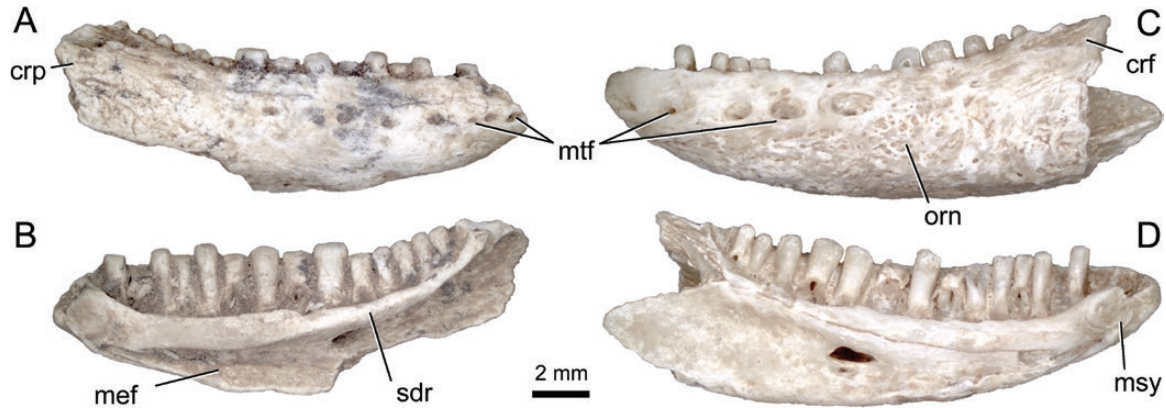


Figure 13. Dentaries and splenial of *Timon* sp. in lateral (A, C) and medial (B, D) views. (A, B) MT-IX-055; (C, D) MT-IX-056. Note the distinct separation between enlarged central and small distal teeth, and the large number of the latter in MT-IX-055. Abb.: crf, coronoid facet; crp, coronoid process; mef, Meckelian fossa; msy, mandibular symphysis; mtf, mental foramina; orn, ornamentation; sdr, subdental ridge.

and the posteromedial processes is relatively narrow (approximately 50°), which was considered typical for Lacertinae by Čerňanský *et al.* (2016). The anteromedial and labial processes have flat internal and external surfaces. The coronoid process is marked by a weakly elevated ridge on the lateral surface, which extends along its anterior margin. The lateral side of the coronoid process is ventrally bound by a slightly curved surangular margin, which separates the process from the articular facet for the surangular on the posteromedial process. This facet bears an oblique striation. The medial surface of the coronoid process bears a distinct, vertical prearticular crest on the posterior portion, followed posteriorly by a variably deep facies coronoideus (*sensu* Rauscher, 1992; Fig. 14A).

Variability: The anterior margin of the coronoid process is sinuous in the smaller two elements and straight in the largest one. The summit is, therefore, also more pointed in the largest element and somewhat more anteroposteriorly elongate in the smaller two. The posterior concavity increases in depth from the smallest to the largest coronoid.

Compound bone

Preservation: Two left elements are preserved, but lack most of the part composed of the surangular, and the anterior tips. The largest element (Fig. 15) has a preserved anteroposterior length of 13.7 mm.

Morphology: The bones form the posterior portion of the central edge of the mandible and its posterior end bearing the retroarticular process, and the posterior portion of the ventral edge. The lateral side is formed by a thin bony wall, which bears the facet for the angular laterally (Fig. 15B). This facet has a pointed posterior

end and a straight ventral margin, which extends anteroventrally from the posterior tip to participate in the ventral edge of the mandible. The dorsal surface of the compound bone is transversely concave medial to the lateral wall. This concavity is medially bordered by a weakly developed longitudinal ridge, which connects to the anteromedial corner of the articular surface for the quadrate. The ventral surface is rounded anteriorly and converges into a distinct crest below the retroarticular process. The retroarticular process bears the articular facet for the quadrate anteriorly and an elongate, well-developed sulcus posterior to it (Fig. 15A). The articular surface faces posterodorsally and forms the widest point of the process, which continuously tapers towards a rounded posterior tip. Its lateral margin is straight, whereas the medial margin is slightly sinuous in dorsal view. A small foramen pierces the longitudinal sulcus (Fig. 15A). The sulcus is medially and laterally bordered by distinct crests, the lateral one being more elevated than the medial one. The medial crest projects more transversely than the lateral crest, resulting in a deeper concavity on the medial surface of the retroarticular process, compared to the flatter lateral surface.

Variability: There is some variability in the development of the ventral crest below the retroarticular process.

Osteoderms

Preservation: None of the osteoderms is preserved completely. The largest reaches 11.4 mm, probably in anteroposterior length.

Morphology: Given that none of the elements is preserved completely, it is difficult to distinguish them. At least some of the osteoderms might represent

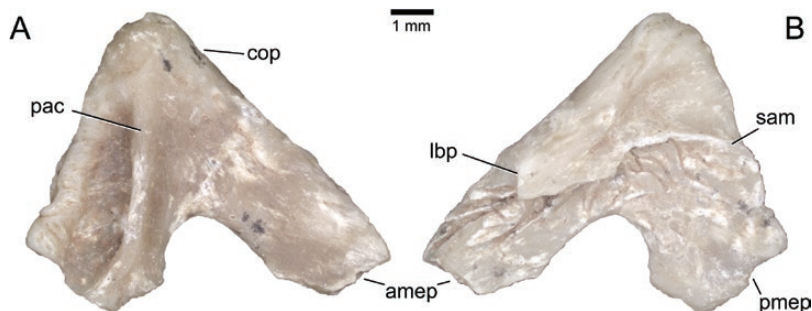


Figure 14. Left coronoid of *Timon* sp. (MT-IX-057) in medial (A) and lateral (B) views. Abb.: amep, anteromedial process; cop, coronoid process; lbp, labial process; pac, prearticular crest; pmep, posteromedial process; sam, surangular margin.

supraocular ones. As is typical for osteoderms, they have a smooth internal and a rugose external surface. They are variably convex externally.

Tooth-bearing bones: Several fragments of tooth-bearing bones are very poorly preserved, so that it is not possible to establish if they belong to maxillae or dentaries. However, the morphology of their teeth is comparable to that of the above-described maxillae and dentaries.

POSTCRANIAL SKELETON

Presacral vertebrae

Preservation: The vertebrae are generally well-preserved, but most of them lack the neural spine summit. Only one intercentrum is preserved in parts, fused to one of the axes. Measurements are provided in the [Supporting Information](#).

Morphology: Presacral vertebrae, including both cervical and dorsal ones, are robust. They are procoelous and more or less anteroposteriorly elongated. Cotyle and condyle are subcircular or slightly ellipsoid, and a distinct groove occurs around the base of the condyle.

The axes are all fused with the odontoid process, and have thus biconvex centra ([Fig. 16](#)). The anterior articular surface is wider than tall. Due to the anteriorly projecting odontoid process on the dorsal part of the facet, the entire surface is dorsoventrally concave. Two small fossae mark the dorsal surface of the odontoid process. The lateral surface of the centrum is anteroposteriorly concave and dorsally bordered by a distinct posterior centrosynapophyseal lamina (PCYL; *sensu* [Tschopp, 2016](#)). Ventrally, the lateral surface curves gently into the ventral surface, which bears a weak, but distinct longitudinal keel along its midline. This keel connects the base of the second intercentrum anteriorly with the base of the third intercentrum (which is broken off) posteriorly. Where preserved, the intercentrum does not have an anterior projection

and extends posteroventrally. The lateral surfaces of the intercentrum are marked by weak crests, which connect the ventral blade with the vertebral centrum, and which bear small, subtriangular posterior projections to the left and to the right of the ventral blade ([Fig. 16E](#)). The synapophysis always lacks the tip, but it is clear that it forms a distinct process projecting posterolaterally. It is anteriorly supported by a short anterior centrosynapophyseal lamina (ACYL). The dorsal surface of the centrum forms the floor of the neural canal. It bears a continuous, longitudinal ridge along its midline, separating two elongate concavities within the neural canal. The posterior condyle is slightly taller than wide, but otherwise nearly hemispherical. The pedicels of the neural arch have concave anterior and posterior margins, which are formed by thin centroprezygapophyseal (CPRL) and centropostzygapophyseal laminae (CPOL), respectively. The CPRL are oriented subvertically, supporting the prezygapophyses. The prezygapophyses themselves are not preserved. The CPOL support the

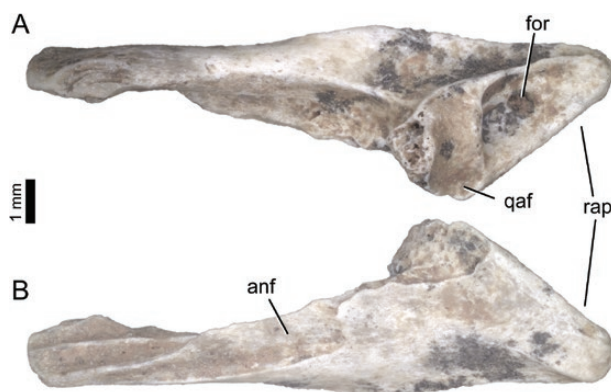


Figure 15. Posterior portion of a left compound bone of *Timon* sp. (MT-IX-058) in dorsal (A) and lateral (B) views. Abb.: anf, angular facet; for, foramen; qaf, quadrate articular facet; rap, retroarticular process.

postzygapophyses, which have transversely concave articular facets. Medial to the facets, there are distinct zygantra. The postzygapophyses are connected with the synapophyses by a weak postzygosynapophyseal lamina (POYL), and with the prezygapophyses through a weak postzygoprezygapophyseal lamina (PPRL) (Fig. 16B). The neural spine is supported by the spinoprezygapophyseal lamina (SPRL) anteriorly and the spinopostzygapophyseal lamina (SPOL) posteriorly. It has a horizontal spine summit towards its posterior tip, and curves ventrally at its anterior end. It is transversely wider at its posterior end than anteriorly. A weak longitudinal groove extends along the midline on the ventral surface from the posterior to the anterior end of the neural spine, thereby marking also the roof of the neural canal.

The non-axial presacral vertebral centra of the largest vertebrae bear a distinct ventral keel on the ventral surface (Fig. 17B, G). The synapophyses are small and rounded, and slightly dorsoventrally elongated, especially in the cervical vertebrae. The PCYL is always present and distinct, and often bifurcates anteriorly, with a ventral branch connecting to the synapophysis and a dorsal branch connecting to the prezygapophysis (Fig. 17H). The neural canal is subpentagonal and slightly larger than the cotyle in anterior view (Fig. 17D, I). A distinct zygosphene is present on the anterior margin. Pre- and postzygapophyses are wide, suboval and tilted dorsally by approximately 30°. The

neural arch is slightly transversely constricted around midlength, between the pre- and the postzygapophyses, which are connected with each other by a PPRL (Fig. 17C). The postzygapophyses extend far more posteriorly than the neural canal pedicels, and also somewhat more than the centrum. The prespinal lamina (PRSL) is strongly concave in lateral view and is more inclined than the posterior edge of the neural spine at its base, although they become nearly parallel towards the spine summit. Here, the PRSL bears a short anterior projection in some elements. The PRSL and the neural canal floor form an angle that is always greater than 40°. The lateral surface of the post-axial, presacral neural spine also bears a SPRL, which extends from the prezygapophyseal facets towards the summit of the spine. The presence of an SPRL has previously only been recognized in the axis, in which it appears to form the structural equivalent to the TPRL in post-axial vertebrae (Tschopp, 2016). However, weak SPRLs also occur in post-axial vertebrae of the large-sized lacertid *Timon lepidus* MDHC 216, alongside well-developed TPRLs.

Variability: The vertebrae differ in elongation and other ratios, but this can be attributed to serial variation along the vertebral column. Lacertid presacral vertebrae are generally short in the anterior cervical region, become more elongate towards the middle of the dorsal series and decrease abruptly in

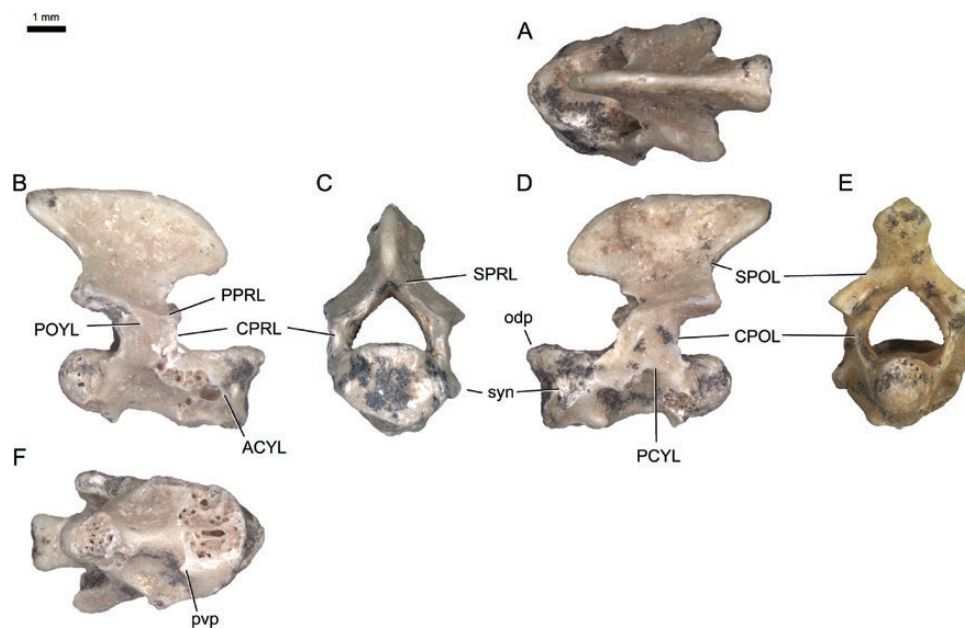


Figure 16. Axis of *Timon* sp. (MT-IX-059) in dorsal (A), right lateral (B), anterior (C), left lateral (D), and ventral (E) views. Abb.: ACYL, anterior centrosynapophyseal lamina; CPOL, centropostzygapophyseal lamina; CPRL, centroprezygapophyseal lamina; odp, odontoid process; PCYL, posterior centrosynapophyseal lamina; POYL, postzygosynapophyseal lamina; pvp, posteroventral projection; SPOL, spinopostzygapophyseal lamina; SPRL, spinoprezygapophyseal lamina; syn, synapophysis.

length in the last two to three elements before the sacrum (Hoffstetter & Gasc, 1969).

Sacral vertebrae

Preservation: None of the sacra is complete. Most of them lack parts of their pleurapophyses. The most complete sacrum has a total width across the pleurapophyses of 12.9 mm.

Morphology: The smaller sacral vertebrae are single, whereas the larger elements are fused (Fig. 18). The centra are procoelous as in the presacral vertebrae. The ventral surfaces of the centra lack a distinct longitudinal keel. The pleurapophyses have distinct ACYL and prezygosynapophyseal laminae (PRYL) and weakly developed PCYL and POYL in the sacral vertebra 1, whereas the opposite is the case in sacral vertebra 2. The pleurapophyses of the two sacral vertebrae tend to fuse at their lateral ends in large individuals, and both are oriented obliquely towards each other, such that their point of fusion is in line with the boundary of the two centra in ventral view (Fig. 18C). The first element has very distinct and widely spread prezygapophyses, and a well-developed zygosphene, whereas all the other zygapophyses in the sacrum are reduced, and no zygantrum is present in the second vertebra. The neural spine is less elevated compared to the most complete presacral vertebrae. A distinct postspinal lamina (POSL) marks the neural spine of the second sacral vertebra.

Variability: Other than the degree of fusion, and differences between sacral vertebrae 1 and 2, no significant variability could be observed.

Caudal vertebrae

Preservation: The material has an overall good status of preservation, though the transverse processes and the neural spines often lack their distal ends. The largest, well-preserved caudal vertebra has a total dorsoventral height of 6.2 mm.

Morphology: The anterior, non-autotomic caudal vertebrae are large with long and laminar transverse processes (Fig. 19A–E). In all specimens, the cotyles and condyles have a rounded outline. There are no distinct pedicels for the chevrons on the ventral surface of the vertebral centra. The neural canal is slightly larger than the centrum. The neural canal is triangular, both in anterior and in posterior view. The zygosphene is scarcely developed, laterally bordered by the two symmetrical prezygapophyseal facets, which are dorsoventrally slanted and anterolaterally directed. Posteriorly, the postzygapophyses are somewhat smaller and more medially directed than the prezygapophyses. Pre- and postzygapophyses are interconnected with a distinct PPRL, especially in more posterior, non-autotomic caudal vertebrae (Fig. 19C). The neural spine is greatly elevated in the anterior-most elements

Autotomic caudal vertebrae (Fig. 19F–N) have sub-parallel transverse processes on both halves, with the posterior ones being shorter than the anterior ones (corresponding to ‘Pattern B’ of Arnold, 1989). The centra are elongate and procoelous. There is a distinct PCYL, but no PPRL. In contrast to the non-autotomic vertebrae, autotomic elements also have a distinct interpostzygapophyseal lamina (TPOL) bordering

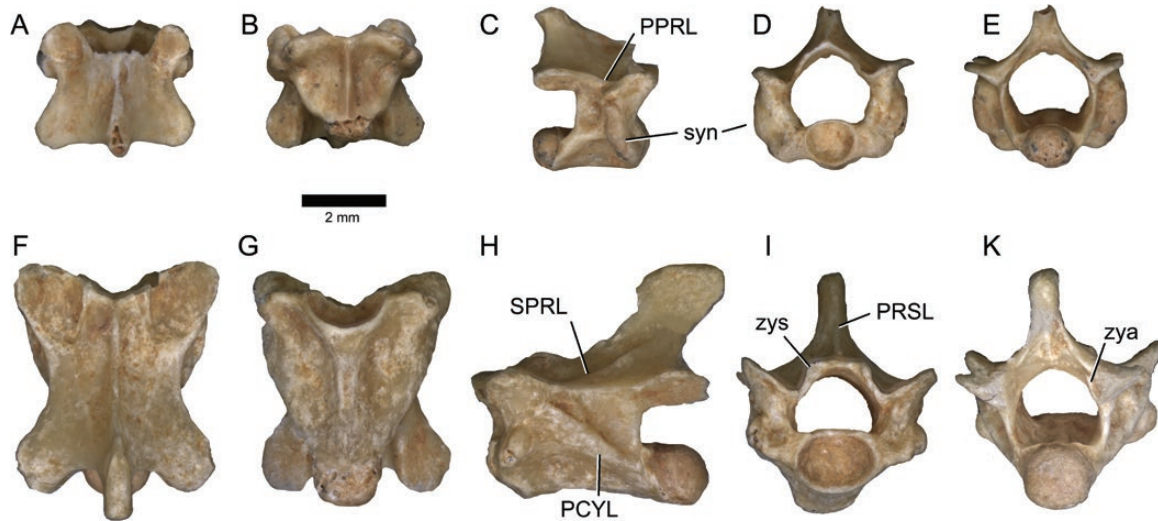


Figure 17. Presacral vertebrae MT-IX-020 (cervical: A–E) and MT-IX-029 (dorsal: F–K) of *Timon* sp. in dorsal (A, F), ventral (B, G), lateral (C, H), anterior (D, I), and posterior (E, K) views. Abb.: PCYL, posterior centrosynapophyseal lamina; PPRL, postzygapoprezygapophyseal lamina; PRSL, prespinal lamina; SPRL, spinoprezygapophyseal lamina; syn, synapophysis; zya, zygantrum; zys, zygosphene.

a deep fossa below the neural spine summit, as in *Podarcis waglerianus* MDHC 390 (Tschopp, 2016). The neural spine is marked by a POSL.

Variability: The caudal vertebrae vary in the inclination of the spine and the orientation of the transverse processes, but this can be attributed to different serial positions along the column (Etheridge, 1967).

Scapulocoracoid

Preservation: A single, left scapulocoracoid is present among the material from the site IX-*Prolagus*. It lacks the dorsal portion of the scapula, the ventral half of the coracoid and the procoracoid (Fig. 20A). The preserved dorsoventral length is 10.8 mm.

Morphology: The scapulocoracoid is convex dorsoventrally in axial view. No suture is visible between the scapula and the coracoid. The scapular blade has subparallel anterior and posterior margins close to the glenoid surface, but appears to expand anteroposteriorly towards its dorsal end, which is broken off. A distinct, elevated, dorsoventrally elongate facet is located on the posterior margin, close to the glenoid fossa. The cross-section of the scapular blade is oval, with a pointed anterior corner and a transversely wider posterior portion. The glenoid fossa is saddle-shaped, being convex anteroposteriorly and concave dorsoventrally. The scapular portion of the glenoid fossa is wider than the contribution from the coracoid. The coracoid is marked by two distinct depressions, one between the procoracoid and the mesocoracoid, where also the supracoracoid foramen is located (Fig. 20A). The second concavity lies ventral to the mesocoracoid, but due to its incompleteness, it remains unclear if there could have been a distinct emargination as in teiids (Lécuru, 1968; Estes, de Queiroz & Gauthier, 1988). The coracoid foramen is located at about the centre of the glenoid facet.

Humerus

Preservation: Most of the humeri are in a good preservational status, even if some lack either the distal or the proximal end. The most complete humerus is MT-IX-017 (Fig. 20B, C), and has a proximodistal length of 18 mm.

Morphology: These bones have a long and slender shaft. The proximal end, when preserved, is of subequal width to the distal one. The proximal epiphysis bears a moderately small humeral condyle, flanked by well-developed medial and lateral tuberosities. Two sharp ridges, the humeral (medially) and the deltopectoral crests (laterally), extend distally from the two tuberosities (Fig. 20C). The deltopectoral crest forms a slightly obtuse angle with the rest of the proximal

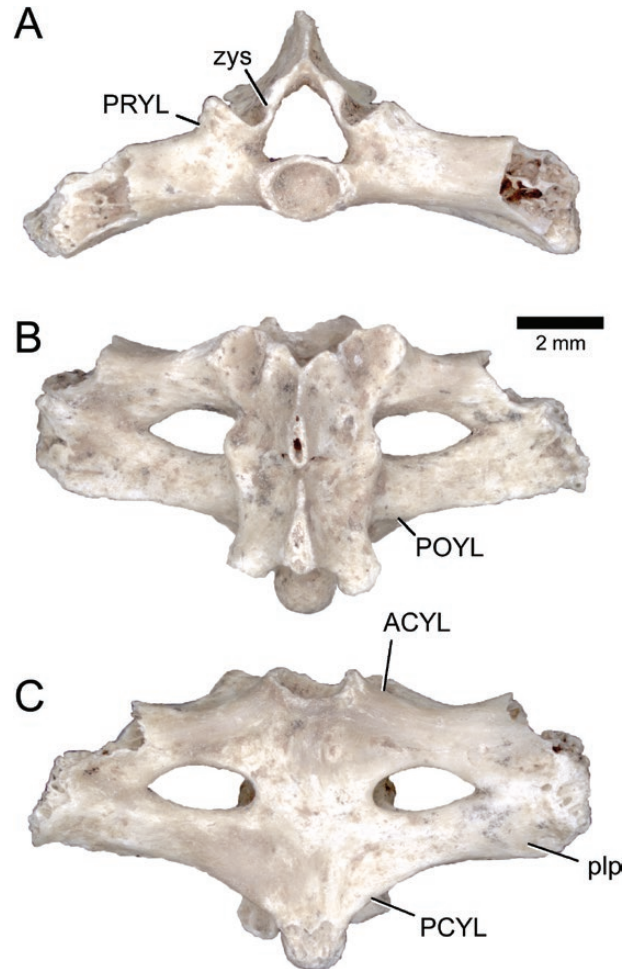


Figure 18. Sacral vertebrae of *Timon* sp. (MT-IX-060) in anterior (A), dorsal (B), and ventral (C) views. Abb.: ACYL, anterior centrosynapophyseal lamina; PCYL, posterior centrosynapophyseal lamina; plp, pleurapophysis; POYL, postzygosynapophyseal lamina; PRYL, prezygosynapophyseal lamina; zys, zygosphene.

end, also forming a very soft dorsal step. In dorsal view, the margin connecting the humeral condyle and the lateral tuberosity is steeply inclined. A moderately deep ventral fossa is present on the ventral surface of the proximal epiphysis (Fig. 20C). The diaphysis is straight, and tends to be dorsoventrally flattened. It forms almost two-fifths of the total length of the humerus. The distal end, when preserved, displays two distinct apophyses, encompassing a complex articular zone. The lateral-most articular part of this zone is represented by the radial condyle, which is transversely compressed. The ulnar condyle is more rounded and slightly larger than the radial condyle. The two condyles are separated by a shallow condylotrochlear gutter and a deep radioulnar fossa is located proximal to them. The ulnar condyle is medially delimited by

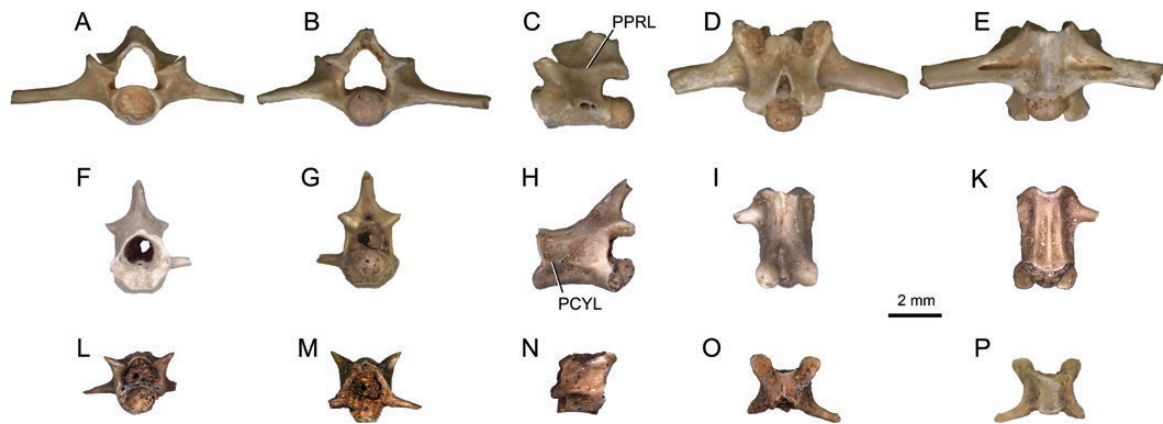


Figure 19. Non-autotomic (MT-IX-019; A–E) and disarticulated autotomic caudal vertebrae (F–I, posterior half, MT-IX-062; K–N, anterior half, MT-IX-061) of *Timon* sp., in anterior (A, F, K), posterior (B, L), left (C, G), and right lateral (M), dorsal (D, H, N), and ventral (E, I) views. Abb.: PCYL, posterior centrosynapophyseal lamina; PPRL, postzygoprezygapophyseal lamina.

the entepicondyle, which reaches further distally than the radial and ulnar condyles. The lateral margin of the distal epiphysis is marked by a weakly developed ectepicondyle. The latter is connected proximally with a sharp ectepicondylar crest and is pierced by the ectepicondylar foramen. There is no entepicondylar foramen.

Ulna

Preservation: One left ulna is preserved completely (Fig. 20D, E). It is 14.2 mm long and has a minimum transverse shaft width of 0.8 mm.

Morphology: The ulna is a slender bone, which curves ventrally and slightly laterally towards its distal end. The proximal end bears the olecranon process, with a proximodistally concave articular facet for the humerus (Fig. 20D). The facet is wide proximally and tapers to a point distally, forming a distinct process projecting medially. A weak ridge follows the curvature of the articular facet posterior to it. The posterior surface of the olecranon process is concave for the reception of the radius, whereas the anterior surface is flat to slightly convex. The shaft is transversely compressed, most strongly around midshaft. Transverse width continuously decreases from proximal to distal, and reaches its minimum length close to the distal articular surface. The distal surface is expanded in anterior view, medially more so than laterally. It bears a semispherical articular surface for the carpals.

Pelvic girdle

Preservation: The pelvic bones are often damaged, in most cases lacking either the pubis or the ischium. The pubis is incomplete in all specimens where it is preserved. In the largest specimens, the maximum diameter of the acetabulum is 4.5 mm.

Morphology: All pelvic girdles are large and composed by completely fused ilium, ischium and pubis (Fig. 21A, B). The acetabulum is large and suboval, with no trace of a suture line. The ilium is long, mediolaterally compressed and posteriorly narrowing. The posterior end is always broken off. Anteriorly, close to the acetabulum, all elements bear a pointed preacetabular process, which projects almost perpendicular to the long axis of the iliac blade (Fig. 21A, B). The dorsal margin of the ilium can show a very low angle in lateral view.

The ischium is triangular, and forms a 90–95° angle with the ilium. The most complete specimens are distinctly enlarged distally to form a wide laminar portion.

As written above, the pubis is almost never preserved, but the wide obturator foramen (or at least its posterior margin) is still visible in some specimens.

Variability: The acetabulum can range from subcircular to rather oval.

Femur

Preservation: Most femurs are almost complete. Only MT-IX-039 lacks the distal epiphysis. The longest and most complete femur, MT-IX-016 (Fig. 21C, D), has a proximodistal length of 24 mm.

Morphology: All specimens preserving both extremities have a long diaphysis forming more than two-thirds of the length of the bone. When preserved, the proximal end bears a well-developed, laterally expanded femoral condyle and on its opposite side lies a smaller, anteriorly directed internal trochanter, separated from the condyle by a deep intertrochanteric fossa in ventral view (Fig. 21D). The shaft is only slightly curved, mostly towards the distal extremity.

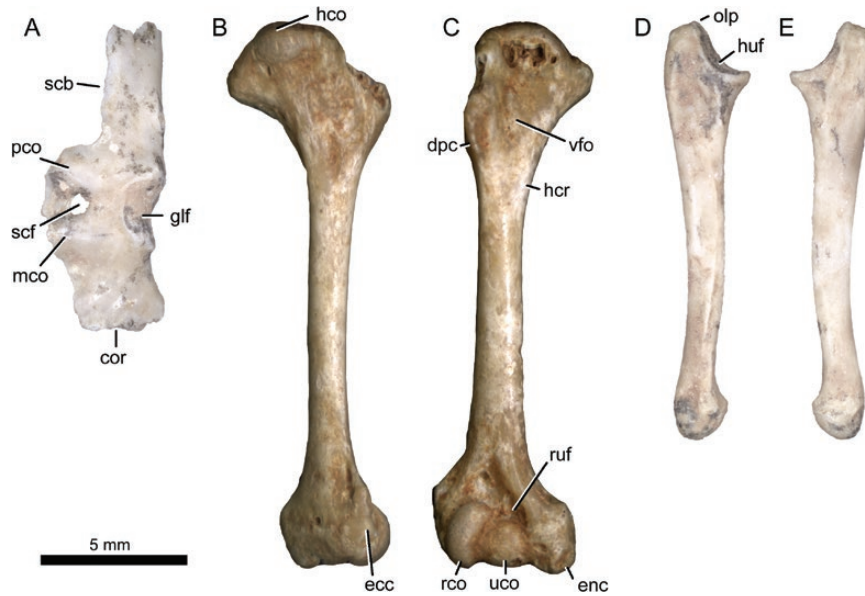


Figure 20. Forelimb elements of *Timon* sp., A, left scapulocoracoid MT-IX-063 in ventrolateral view; B, C, right humerus MT-IX-017 in dorsal, B, and ventral, C, views; D, E, left ulna MT-IX-064 in posterior (D) and anterior (E) views. Abb.: cor, coracoid; dpc, deltopectoral crest; ecc, ectepicondyle; enc, entepicondyle; glf, glenoid fossa; hco, humeral condyle; hcr, humeral crest; huf, humeral articular facet; mco, mesocoracoid; olp, olecranon process; pco, procoracoid; rco, radial condyle; ruf, radioulnar fossa; scb, scapular blade; scf, supracoracoid foramen; uco, ulnar condyle; vfo, ventral fossa.

There is no linea aspera on the ventral surface of the shaft, which divides the ventral origin of the *M. femorotibialis* in iguanids (Russell & Bauer, 2008). The distal epiphysis is composed by a well-developed posterior condyle and by a smaller anterior condyle. The related small epicondyles are located proximally to each condyle. In ventral view, the intercondylar groove is very shallow, as well as the popliteal fossa (Fig. 21D). In dorsal view, a low and sharp ridge is visible on the anterior portion of the epiphysis.

Tibia

Preservation: Most of the recovered tibiae are preserved completely, but some lack their distal end. The longest element has a proximodistal length of 19.3 mm.

Morphology: The tibia is straight in dorsal view and slightly curved in anterior view (Fig. 21E, F). The proximal epiphysis bears two subparallel condyles for the articulation with the femur. A distinct cnemial crest extends ventrally from the posterodorsal corner of the articular surface for about one-fifth of the entire proximodistal length of the tibia (Fig. 21F). A ventral crest marks the anteroventral edge of the shaft approximately at the level, where the cnemial crest fades out. The dorsal surface of the shaft between the two crests is slightly concave anteroposteriorly. The ventral crest bears a small tubercle for the insertion of the *M. femorotibialis gastrocnemius* (Russell & Bauer, 2008). At midshaft, the diapophysis has a subtriangular cross-section, with a flat dorsal and a

pointed ventral surface. The distal portion of the shaft is marked by a distinct tubercle for the insertion of the distal tibiofibular ligament (Russell & Bauer, 2008). This tubercle is located on the anterodorsal edge of the distal shaft. The distal articular surface is oval in distal view, being taller dorsoventrally in its posterior half. The anterior portion of the articular surface projects further distally than the posterior one.

Astragalocalcaneum

Preservation: The only preserved tarsal bone (MT-IX-066; Fig. 21G, H) is complete. It has a maximal transverse width of 6.1 mm.

Morphology: The astragalocalcaneum has two distinct articular surfaces for the tibia and fibula. The facet for the tibia is transversely convex and curves somewhat on to the medial surface of the bone. The fibular facet is dorsoventrally narrower than the tibial one and transversely concave (Fig. 21G, H). The two facets are separated by a groove and well offset from the rest of the bone. A dorsoventrally compressed bony shelf projects laterally, forming the lateral margin of the element. The medial margin is subparallel to the lateral one, but taller dorsoventrally, and bears a short longitudinal ridge on the anteroventral edge. The dorsal surface is transversely convex anterior to the fibular facet and concave anterior to the tibial facet. The ventral surface is relatively uniform. The distal surface is irregularly sinuous, bearing the facets for the distal tarsals.

Metapodial

Preservation: The four preserved metapodials are nearly complete. The longest has a proximodistal length of 12.6 mm and a minimum shaft width at midshaft of 0.9 mm.

Morphology: The four bones are probably all from different positions in the manus or pes, but their exact identity could not be established. They have an elongate shaft, with expanded proximal and distal ends (Fig. 21I–K). The proximal ends are expanded more widely than the distal ones, and bear concave articular facets, whereas the distal surface bears condyles for the articulation of the phalanges.

Variability: There is some variability in the expansion of the proximal articular surfaces, but this is probably due to the different positions in the manus or pes.

ATTRIBUTION TO A SINGLE SPECIES

All the fossil material from Monte Tuttavista referred to *Lacerta* sp. by Abbazzi *et al.* (2004), and later by one of us (M. Delfino), is herein considered to belong to a single species. This attribution is supported by several lines of evidence. First, lacertid species of comparable size to the fossil material studied herein (i.e. large species of *Gallotia* and *Timon*) do not generally have overlapping species ranges today (Barahona *et al.*, 2000; Ahmadzadeh *et al.*, 2016), indicating that mutual exclusion patterns occur at a certain size. There is only one case of a narrow contact zone between *Timon lepidus* and *T. nevadensis* in Spain, which probably resulted from a secondary contact (Miraldo *et al.*, 2013; Ahmadzadeh *et al.*, 2016). Second, the variable osteological features in the single elements discussed in the Description can be explained by a combination of

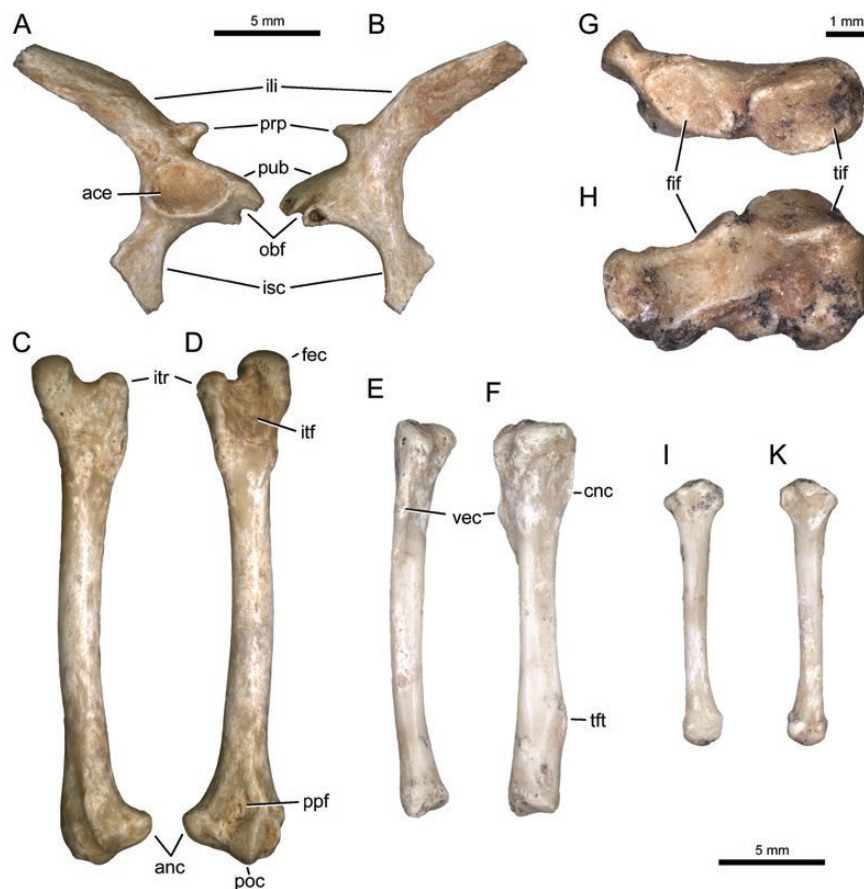


Figure 21. Hindlimb elements of *Timon* sp., A, B, right coxal bone MT-IX-018 in lateral (A) and medial (B) views; C, D, right femur MT-IX-016 in dorsal (C) and ventral (D) views; E, F, right tibia MT-IX-065 in anterior (E) and ventral (F) views; G, H, left astragalocalcaneum MT-IX-066 in proximal (G) and dorsal (H) views; I, K, metapodial, views uncertain. The 5 mm scale bars are valid for the elements figured in A–F and I–K. The 1-mm scale bar is valid for the astragalocalcaneum. Abb.: ace, acetabulum; anc, anterior condyle; cnc, cnemial crest; fec, femoral condyle; fif, fibular articular facet; ili, ilium; isc, ischium; itr, intertrochanteric fossa; ift, internal trochanter; obf, obturator foramen; poc, posterior condyle; ppf, popliteal fossa; prp, preacetabular process; pub, pubis; tft, tibiofibular tubercle; tif, tibial articular facet; vec, ventral crest.

patterns. Some cases can be attributed to ontogenetic or size-related changes (see above). In the majority of other cases, variability among the fossil material was also found to be variable within the studied extant species, implying that they stem from individual variation. Finally, dentition and ornamentation are similar in all cranial bones. Therefore, it appears most plausible that only one large-sized lacertid species occurs in the Pleistocene of Monte Tuttavista.

PHYLOGENETIC ANALYSIS

METHODOLOGY

The phylogenetic analysis is based on an updated version of the matrix used for the *Lacerta* case study in Villa *et al.* (2017). Some characters were added based on literature (Hoffstetter & Gasc, 1969; Lécureu, 1968, 1969; Estes *et al.*, 1988; Al-Hassawi, 2004; Arnold *et al.*, 2007; Bailon *et al.*, 2014; Čerňanský *et al.*, 2016) and on personal observations of additional specimens studied in the meantime.

Taxon sampling has been adapted such that specimen-level operational taxonomic units (OTUs) in Villa *et al.* (2017) were collapsed to represent single species (see Supporting Information Table S2 for the list of specimens studied per species, and for additional sources from the literature). Because the material was initially referred to *Lacerta* sp. (Abbazzi *et al.*, 2004), we included all species of *Lacerta*, except for *L. pamphylica* from Turkey, of which no skeletal specimen could be found in any museum collection we contacted for loans or visited personally. In addition, we included all three species-complexes of *Timon*, all lacertid species currently existing on Sardinia and additional representative species of all genera currently living in the surrounding countries (Algeria, France, Italy, Spain and Tunisia). We also added two species of *Gallotia* and the fossil lacertid *Maioricalacerta rafelinensis* from the Pliocene of Mallorca (Spain; Bailon *et al.*, 2014), given that they are, or were, large-sized lacertids living on islands, as well as two fossil representatives of Gallotiinae from France and Germany, *Pseudeumeces cadurcensis* and *Janosikia ulmensis* (Augé & Hervet 2009; Čerňanský *et al.*, 2016). The outgroup consists of a teiid (*Salvator merianae*), a scincoid (*Chalcides ocellatus*) and *Varanus exanthematicus*, representing successively more distantly related clades to Lacertidae (Gauthier *et al.*, 2012; Pyron *et al.*, 2013; Reeder *et al.*, 2015). The complete matrix was constructed in MESQUITE (v.3.2, build 801; Maddison & Maddison, 2017), and consists of 223 character statements (156 cranial and 67 postcranial ones) and 36 species-level operational taxonomic units. A MESQUITE file and a TNT input file are provided in the Supporting Information.

In order to include some information concerning intraspecific variability, we used majority scoring for polymorphic characters, or polymorphic scores in cases where an equal number of specimens was scored for conflicting character states (*sensu* Wiens, 1995, 1998, 2000).

The fossil material from Orosei has been scored as a single, combined OTU, assuming that there was only one large-sized lacertid (see above). The fossils were not scored for quantitative characters that code for ratios between different bones or average ratios of a series of vertebrae, because a correct scoring of these characters depends on a consistent use of vertebrae from similar serial positions throughout the presacral column, and requires that the bones to be compared are from the same individual. Given that this could not be guaranteed due to the disarticulated and incomplete state of the fossil material, we refrained from scoring these quantitative characters. The measurements and consequential number of single elements scorable for a specific quantitative character state are provided in the Supporting Information.

The phylogenetic analysis was performed with TNT v.1.1 (Goloboff, Farris & Nixon, 2008), under equal weighting. Meristic and quantitative multistate characters, as well as discrete ones that code for an obvious morphocline, were treated as ordered, following Brazeau (2011). We used the New Technology Searches, using all available algorithms with their default settings, and stabilizing the consensus tree five times with a factor of 75. After a first iteration of tree searches, the resulting shortest trees were taken as a starting point for a second round of tree bisection and reconnection, in order to find all possible shortest trees.

RESULTS

A first, unconstrained analysis yielded four most-parsimonious trees of a length of 1000 steps. However, the strict consensus tree did not retrieve the monophyly of several clades that have repeatedly been found as such by the latest phylogenetic analyses based on molecular studies. These include Lacertinae and Lacertini (Arnold *et al.*, 2007; Kapli *et al.*, 2011), and the genera *Algyroides* (Mendes *et al.*, 2016), *Iberolacerta* (Carranza *et al.*, 2004; Mendes *et al.*, 2016), *Lacerta* (Carranza *et al.*, 2004; Sagonas *et al.*, 2014; Marzahn *et al.*, 2016; Mendes *et al.*, 2016) and *Podarcis* (Carranza *et al.*, 2004; Carretero, 2008; Mendes *et al.*, 2016), which were all recovered as paraphyletic in the unconstrained search herein. Therefore, we reran the analysis with seven a priori constraints, in order to find the generally accepted basic structure of the phylogenetic tree. Given that the phylogenetic position of the extinct species *Pseudeumeces cadurcensis*, *Janosikia*

ulmensis, *Maioricalacerta rafelinensis* and the OTU representing the material from Sardinia described herein could not be confirmed with molecular analyses, we defined these species as wild-card taxa. This means that they were excluded from the defined constraints, and could thus be recovered anywhere in the tree by the analysis. The monophyly constraints implemented in this second iteration of the analysis were defined for Gallotiinae (*Gallotia* and *Psammodromus*), Lacertinae (Eremiadini and Lacertini), Lacertini (*Algyroides*, *Archaeolacerta*, *Iberolacerta*, *Lacerta*, *Podarcis*, *Timon* and *Zootoca*), as well as the genera *Algyroides*, *Iberolacerta*, *Lacerta* and *Podarcis*. Other than for these constraints, the methodological details for this second iteration remained the same as in the first one.

The second iteration found 19 constrained trees with a minimum length of 1040 steps – 40 steps more than the unconstrained searches (corresponding to an increase in tree length of 4%). As in the study of Čerňanský *et al.* (2016), *Pseudeumeces cadurensis* and *Janosikia ulmensis* are recovered within the clade Gallotiinae, as is *Maioricalacerta rafelinensis*. The material described herein is recovered as the sister-taxon to the three species-complexes of *Timon* (Fig. 22).

The following synapomorphies recovered for Lacertidae also occur in the fossil material from Monte Tuttavista: (1) frontals with an anterior transverse width that is greater than 1.2 times the minimum transverse width (at least in the majority of the preserved frontals, see Supporting Information Table S4); (2) a subrectangular dorsal, ornamented surface of the parietal; and (3) a weakly developed pterygoid recess. Potential synapomorphic features supported in some, but not all, topologies found, and shared by most lacertid species and the taxon described herein, include a well-developed dermal ornamentation on the parietal, with distinct, symmetrical grooves delimiting the scutes. Other features mentioned as possibly diagnostic characters for Lacertidae in the literature (e.g. Hoffstetter 1944; Augé *et al.*, 2003; Bailon *et al.*, 2014), which are present in the material described herein, are (1) generally arched dentaries with a continuously widening Meckelian fossa extending from the symphysis backwards; (2) a well-developed splenial facet on the subdental ridge of the dentary, which reaches close to the symphysis; (3) the presence of a distinct coronoid facet on the postero-dorsal portion of the labial surface of the dentary; and (4) a well-developed carina maxillaris on the medial surface of the facial process of the maxilla.

An attribution to Lacertinae is supported by the absence of pedicels for the chevrons on the caudal vertebrae. Potential synapomorphies of Lacertinae found in some topologies are the absence of an anterior or anterodorsal projection on the anterior margin of the

facial process of the maxilla and the presence of a short, longitudinal ridge on the dorsomedial portion of the central pillar of the quadrate.

The dorsoventral constriction in the ascending nasal process of the premaxilla was found as a synapomorphy for Lacertini. Additional, potentially synapomorphic features for this clade include the maximum number of cusps in any tooth being three and a large maxillary facet on the lateral surface of the jugal.

The fossil material described herein shares the following synapomorphies of the clade uniting *Timon* and *Lacerta*: (1) the presence of pterygoid teeth; (2) the splenial reaches far anteriorly. Synapomorphies of this clade found in some but not all topologies, which also occur in the material from Monte Tuttavista, are: (3) a transversely expanded ascending nasal process on the premaxilla; and (4) well-developed parietal tabs that underlie the frontals.

Nine synapomorphies unite the material from Monte Tuttavista with the extant species of *Timon*. None of them is exclusive to this clade and all of them also occur in individuals of some species of *Lacerta*. However, the combination of these traits does not appear like this in any of the studied specimens of extant lacertids. The features are the following: (1) the maxillary tooth row curves laterally towards its posterior end (this feature also occurs in *Lacerta media* and some specimens of *L. trilineata*); (2) postfrontal and postorbital are fused (also present in *L. schreiberi*); (3) a concave anterior platform on the quadrate (shared with *L. schreiberi*, although in the latter species, the concavity is much less developed compared to *Timon* and the specimens of Monte Tuttavista); (4) the fossa triangularis and the parietal fossa on the ventral surface of the parietal are connected by a narrow bony ridge (also present in large-sized species of *Lacerta*); (5) long paroccipital processes (also present in large-sized species of *Lacerta*); (6) a mushroom-shaped basioccipital (variable within *Lacerta*); (7) a flat to weakly concave anterior portion of the lateral surface of the splenial (shared with *L. bilineata* and *L. strigata*); (8) the teeth overtop the dental crest of the dentary by less than half the height of their crown (variable within *Lacerta*); and (9) short posterior projections lateral to the ventral keel on the axial intercentrum (occurs as well in *L. trilineata*, *L. viridis* and some *L. schreiberi*). Two additional potential synapomorphies were found by some, but not all, topologies: (1) a weak pterygoid recess; and (2) a distinct symphyseal facet on the dentary. Whereas the latter character seems relatively constant, the weak pterygoid recess is also found as synapomorphic for Lacertidae, shows a reversal in a basal node within Lacertini, close to the split with Eremiadini and remains variable within *Timon* and *Lacerta*, so that we refrain from considering this feature as taxonomically useful within Lacertini.

The Monte Tuttavista lacertid can be excluded from *Lacerta* because individuals of the latter genus generally have (1) a reduced or no maxillary facet on the frontal for the anterior prefrontal process of the maxilla (except for *L. trilineata* and some specimens of *L. bilineata*); (2) no dorsoventral constriction of the ascending nasal process of the premaxilla (except for *L. trilineata* and some specimens of *L. viridis*); and (3) straight articular facets of the postzygapophyses (with the exception of *L. trilineata* and some specimens of *L. media*). Although these traits are variable within *Lacerta*, no variability could be observed in the fossil material. An additional feature usually cited as diagnostic for the genus *Lacerta* is a step-like morphology of the dorsal margin of the posterior process of the maxilla. Such a step is lacking in all maxillae from Monte Tuttavista studied herein, further arguing against a referral of this material to the genus *Lacerta*. However, the dorsal margin of the posterior process of the maxilla can have a series of different morphologies also within the genera *Lacerta* and *Timon*. In the latter, most specimens have an incipient, rounded step, as also occurs in *L. schreiberi*. Specimens of other *Lacerta* species have a more distinct step, forming a sharp, nearly right-angle (e.g. *L. strigata*), or even bear a posteriorly projecting spur (e.g. *L. trilineata*). Because of the variability of this feature, it remains unclear if it can be interpreted as a diagnostic feature of *Lacerta*, but it can certainly be used to distinguish the material described herein from this genus.

It is interesting to note that, although phylogenetic analysis finds the lacertid from Monte Tuttavista outside *Lacerta*, several traits are shared with one *Lacerta* species in particular: the large-sized *L. trilineata*. Nonetheless, the two species can also be distinguished based on numerous features: (1) the position of the sulcus delimiting the frontoparietal shield on the dorsal surface of the frontal is situated more anteriorly in *L. trilineata* than in the fossil material; (2) the medial ridge on the ascending nasal process of the premaxilla is more strongly developed in the fossil material compared to *L. trilineata* and forms a posterior projection instead of fading out posterodorsally; (3) the maxillary facet on the premaxilla is larger in the material from Monte Tuttavista than in any species of *Lacerta*; (4) *L. trilineata* has significantly more maxillary teeth than the fossil material; (5) there is no step on the posterior process of the maxilla in the Monte Tuttavista lacertid; (6) the articular facet for the palatine on the suprudental shelf of the maxilla is more distinct in the fossil material than in *L. trilineata*; (7) the fossil frontals are mostly fused, whereas frontals of *L. trilineata* generally remain separate throughout their life; (8) *L. trilineata* does not bear a subtriangular anterior projection on the postfrontal; (9) the lateral shield covers more of the postfrontal in the fossil material compared to *L. trilineata* and most other species of *Lacerta*; (10) *L. trilineata* lacks a medial process on the medial ridge of the jugal; (11) differences in

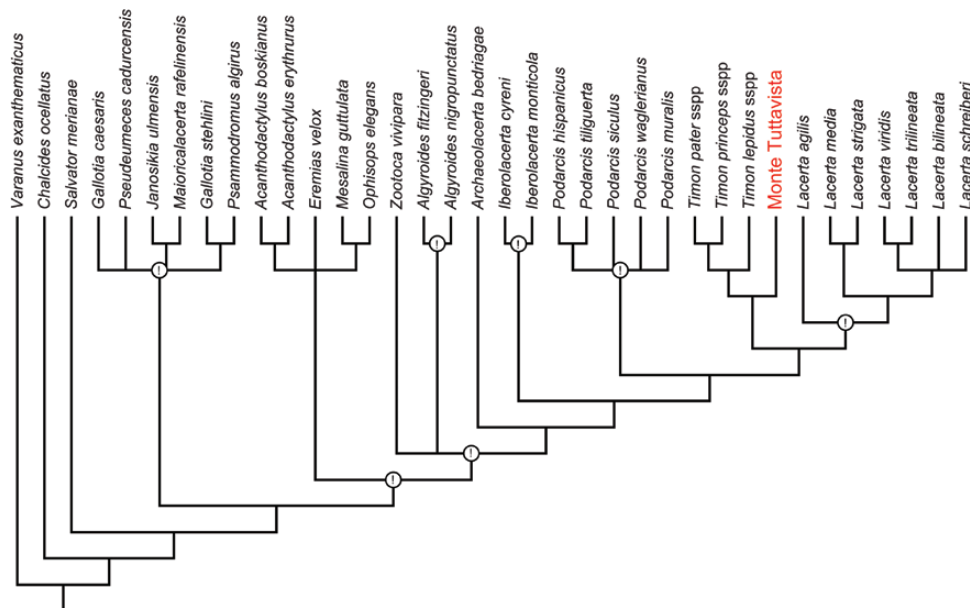


Figure 22. Strict consensus tree calculated from 19 trees constrained to find the accepted higher-level systematic grouping based on molecular data (nodes with exclamation mark). The four extinct taxa *Janosikia ulmensis*, *Maioricalacerta rafelimensis*, *Pseudeumeces cadurcensis* and the fossil material from Monte Tuttavista were treated as wild-card taxa, so that they could be found in any phylogenetic position. The large-sized Monte Tuttavista taxon is recovered as sister-taxon to all extant species of *Timon*, and herein referred to *Timon* sp.

tooth size along the dentary tooth row are much more distinct in the fossil material than in *L. trilineata*, and the tooth row curves dorsally towards its distal end in the former taxon; (12) the coronoid facet is less distinct in *L. trilineata* than in the fossil dentaries and the coronoid process reaches less dorsally, where this feature is preserved; (13) the splenial from Monte Tuttavista has a single posterior end instead of being bifurcated; (14) *L. trilineata* bears a longitudinal ridge in the neural canal floor of the axis, which is interrupted at midlength, whereas it remains distinct throughout its length in the fossil material.

DISCUSSION

TAXONOMIC ASSIGNMENT

Following our phylogenetic analysis, we herein refer the Monte Tuttavista lacertid to *Timon* sp. (in contrast to Abbazzi *et al.*, 2004 who referred it to *Lacerta* sp.), even though it would be equally parsimonious to attribute the material to a new genus, given the sister-taxon relationship of the Monte Tuttavista lacertid with the extant species complexes of *Timon*. We refrain from erecting a new species or genus for this material based on morphological and other reasons. Of the 17 ‘autapomorphies’ recovered by TNT for the Monte Tuttavista lacertid, only one feature results as unique within Lacertidae in the matrix used. This feature is the enlarged articular surface on the tooth-bearing portion of the premaxilla for the anterolateral premaxillary process of the maxilla (Fig. 5F). However, a few individuals of *Timon* (e.g. *T. lepidus* MDHC 216) and *Lacerta* (e.g. *L. bilineata* UAM Q21) also have enlarged facets, but because of the majority scoring used to combine information from multiple individuals into a species-level OTU (see Phylogenetic analysis), these shared morphologies were not represented in the final, species-level matrix. Additionally, a similar morphology of this facet occurs in the extinct lacertid *Dracaenosaurus croizeti* (a premaxilla from Coderet, France; MNHN field number Cod H1-75; E. Tschopp, pers. obs., 2016). Finally, the split between the currently living eastern and western species complexes of *Timon* has been dated to well-before the Pleistocene (Ahmadzadeh *et al.*, 2016), so that the Monte Tuttavista sites fall within the purported lifespan of the genus. A referral of the Monte Tuttavista lacertid to *Timon*, therefore, seems the most reasonable systematic approach to date. Nonetheless, both the geographical distance from current species ranges, and several morphological traits, indicate that the Sardinian material cannot be confidently attributed to any of the extant species or species complexes of *Timon*.

The most significant differences are found in the maxillary dentition and the dentary, indicating that the

Sardinian form had to adapt to a different food source. The ornamentation on the lateral surface and the distinct dorsal curvature of the distal tooth row in some dentaries from Monte Tuttavista could not be observed among individuals of the studied extant species of *Timon*, which also lack the well-defined articular facet for the labial process of the coronoid. Furthermore, in the extant species, the largest maxillary teeth are the caniniform teeth located in the mesial half of the tooth row (Estes & Williams, 1984; Mateo & Lopez-Jurado, 1997), whereas the fossil maxillae often bear greatly enlarged teeth on the distal half of the tooth row. However, these enlarged teeth do not reach the distal-most tooth positions, but are distally followed by a number of distinctively smaller teeth. A similar pattern as in the maxilla also occurs in most fossil dentaries from Monte Tuttavista, which furthermore also have a reduced number of dentary teeth (15–21), especially compared to adult individuals of extant *Timon* species, which reach up to 31 teeth (*T. lepidus* MRAC 3390, E. Tschopp, pers. obs., 2017). Although the number of dentary teeth increases during ontogeny in *Lacerta viridis* (Roček, 1980) and *T. lepidus* (Mateo & Lopez-Jurado, 1997), the difference between the sample from Monte Tuttavista (15–21 dentary teeth) and extant *Timon* (up to 31 dentary teeth) cannot be explained by ontogeny alone, given that many of the largest fossil specimens still bear less than 20 tooth positions. As mentioned in the Description, the most similar dentition to the one found here, occurs in fossil specimens from the Pleistocene of Malta, Sicily and Apulia referred to as ‘*Lacerta*’ *siculimelitensis* (Kotsakis, 1977; Böhme & Zammit-Maempel, 1982; Delfino, 2001). Because of this similarity, and the uncertain taxonomic status of this extinct species (see Mateo, 1988; Barahona & Barbadillo, 1997; Holman, 1998; Delfino & Bailon, 2000), we herein refrain from erecting a new taxon for the Monte Tuttavista lacertid, awaiting a detailed reassessment of ‘*Lacerta*’ *siculimelitensis* (currently in progress). Caution is furthermore warranted concerning the species identification of the Monte Tuttavista material because ‘*L.*’ *siculimelitensis* has been found in equally old strata on the neighbouring island, Sicily, and because some authors proposed that this species might be referable to *Timon* (Mateo, 2009; Ahmadzadeh *et al.*, 2016).

IS *TIMON* SP. FROM SARDINIA AMBLYODONT?

A tendency to enlarged, blunt and molariform teeth has been reported several times in fossil and extant lizards, many of them inhabiting islands. It is very slightly developed in the already mentioned lacertid ‘*Lacerta*’ *siculimelitensis* from Malta and Sicily

(Böhme & Zammit-Maempel, 1982; Holman, 1998). Enlarged, but still pointed, teeth occur in the amphisbaenid *Amphisbaena ridleyi* from Fernando de Noronha in the North Atlantic (Pregill, 1984), whereas strongly enlarged, blunt teeth have been reported in teiids from the Lesser Antilles (Pregill, 1984), iguanids from Cuba (Estes & Williams, 1984), the lacertid *Maioricalacerta* from Mallorca (Bailon *et al.*, 2014) and the anguid *Diploglossus* from Guadeloupe (Bochaton *et al.*, 2016). Some of the enlarged teeth in the maxillae and dentaries attributed to *Timon* sp. herein resemble much the condition of the teeth in *Diploglossus* from Guadeloupe. Often, such a morphology has been described as amblyodonty, referring to Hoffstetter (1944) as defining source for the term. Hoffstetter (1944: p. 549) introduced the term to describe ‘dents arrondies’, rounded teeth. More recently, Čerňanský, Augé & Rage (2015: p. 1) described amblyodonty as ‘blunt and enlarged’ teeth, which seems to be the current general understanding of the term. However, enlarged and blunt teeth are not necessarily rounded, so that it remains unclear to us if amblyodonty means different morphologies to different researchers. Because of this, and because most of the enlarged, rounded teeth in our specimens are worn or damaged, we herein refrain from stating that *Timon* sp. from Sardinia was amblyodont, even though similarities to species often considered to be amblyodont are apparent.

PALEOBIOGEOGRAPHY OF *TIMON*

The herein reported fossils represent the first occurrence of *Timon* in Sardinia, which is outside the current geographical range of the genus, and lies in between the eastern and western areas inhabited by the three distinct species-groups of *Timon* (Ahmadzadeh *et al.*, 2016). However, this is perhaps not so surprising given that, according to distribution models based on current environmental factors, all four western species of *Timon* would be adapted to inhabit Sardinia (Ahmadzadeh *et al.*, 2016). The occurrence of *Timon* in the Pleistocene of Sardinia thus further corroborates a wider distribution of the genus in the recent past, as proposed by Ahmadzadeh *et al.*, (2016).

POTENTIAL CAUSES FOR LOCAL EXTINCTION

Timon is not the only reptile known from Monte Tuttavista that became extinct in Sardinia. The fossil record also documents the presence of agamid lizards, vipers and amphisbaenians (Abbazzi *et al.*, 2004; Delfino *et al.*, 2008; Delfino, Bailon & Pitruzzella, 2011), which are absent on the island nowadays. Other localities from the Miocene and Pliocene testify for the former presence of crocodiles, trionychid turtles, non-*Anguis* anguid lizards, aniliid and erylacine snakes

(Kotsakis, Delfino & Piras, 2004; Delfino *et al.*, 2011; Georgalis *et al.*, 2017).

One of the reasons for local extinction could be the arrival or evolution of new predators. A causal relationship with the first arrival of humans was initially proposed as potential cause for an apparent major faunal turnover during the Pleistocene (Sondaar *et al.*, 1986). Two faunal complexes are recognized based on distinct compositions of the mammalian fauna (the *Nesogoral* and *Microtus* complexes), with two subcomplexes each (Abbazzi *et al.*, 2004; Palombo, 2006, 2009; Palombo & Rozzi, 2014; Vigne, 2014). The findings at Monte Tuttavista confirm the presence of such a turnover (Abbazzi *et al.*, 2004) but more recent data indicate that this turnover has not been as severe as previously thought (Palombo *et al.*, 2017). Also, it currently seems rather improbable that humans really established sustained settlements on the island before the Holocene, which would have been necessary to have such an important impact on the local fauna (Palombo, 2006, 2009; Masini *et al.*, 2008; Leppard, 2014; Palombo *et al.*, 2017). In any case, at Monte Tuttavista, *Vipera* was only found from sites attributed to the *Nesogoral* complex, whereas *Timon* and the agamids occur in both faunal complexes, and only seem to disappear at the beginning of the so-called ‘Dragonara’ subcomplex within the *Microtus* complex (Abbazzi *et al.*, 2004; Palombo, 2006, 2009; Delfino *et al.*, 2008; Palombo & Rozzi, 2014). The extinction of these large lizards does, therefore, not correlate with the main faunal turnover, but rather with the change from the so-called ‘Orosei 2 subcomplex’ to the ‘Dragonara’ subcomplex, confirming a rather gradual faunal change as proposed by Palombo *et al.* (2017).

Whereas an influence of humans on the local extinction of *Timon* and agamids appears unlikely, several carnivore mammals first occur on Sardinia during the ‘Dragonara’ subcomplex. These include three members of Lutrinae, and the small-sized canid *Cynotherium sardous* (Abbazzi *et al.*, 2005; Palombo, 2006, 2009; Palombo & Rozzi, 2014). The lutrines are specialized to prey on aquatic animals (Willemsen, 1992), and can thus probably be excluded as predators of the large lizards. However, the appearance of the endemic canid *Cynotherium sardous* is of particular interest with respect to the extinction of *Timon* and possibly also the vipers and agamids. *Cynotherium sardous* likely evolved from larger canids that first arrived on the island during the Early Pleistocene (just before or during the main faunal turnover: Abbazzi *et al.*, 2005; Lyras & van der Geer, 2006; Lyras, van der Geer & Rook, 2010; Palombo & Rozzi, 2014). Throughout the Pleistocene, these earlier forms became progressively smaller and adapted to prey on small-sized animals like the small lagomorph *Prolagus* (Lyras & van der Geer, 2006; Lyras *et al.*, 2010), and thus possibly also large-sized lizards such as *Timon*, whereas smaller

lizards remained safe from predation by this newly evolved predator (see below). Larger canids, as well as hyaenids, are reported from the early Pleistocene of Sardinia (Rook *et al.*, 2004; Abbazzi *et al.*, 2005; Lyras & van der Geer, 2006), but these were most likely less adapted to feed on smaller prey like *Prolagus*, large lizards and snakes, and became extinct during the faunal turnover (Rook *et al.*, 2004; Palombo, 2006, 2009; Palombo & Rozzi, 2014).

The body size decrease in *Cynotherium*, and thus the evolution of *C. sardous*, can also be traced among the sites at Monte Tuttavista (Abbazzi *et al.*, 2005). Whereas elements attributable to the genus are found nearly throughout all stratigraphic layers, only bones from the two stratigraphically highest sites, 'VI-Banco 6' and 'VII-2', can be tentatively (*C. cf. sardous* at VI-Banco 6; Abbazzi *et al.*, 2005) and definitively referred to the small-sized *C. sardous* (VII-2; Abbazzi *et al.*, 2005). This size decrease apparently correlates, in particular, with the disappearance of *Timon* and agamids: VI-Banco 6 produced six remains attributable to *Timon*, and VII-2 none (see Fig. 1 and Supplementary Material), and the last occurrence of agamids is from 'XI-canide', which is just below the two sites hosting *C. sardous*. Indeterminate snakes and the small-sized, possible *Podarcis* continued to thrive throughout the 'Dragonara' subcomplex, and were among the most frequent finds in VI-Banco 6 (Abbazzi *et al.*, 2004). Around the Pleistocene–Holocene boundary, *Vulpes vulpes* also arrived on Sardinia (Palombo, 2006), which has been shown to prey on lizards and snakes (Díaz-Ruiz *et al.*, 2013).

The Pleistocene was a time of marked climatic oscillations between warmer and colder periods. The end of the Pleistocene corresponds to a cold period (the Younger Dryas; Miraldo *et al.*, 2013), which seems to have had an important impact on the fauna in Corsica (Vigne, 2014) and on the distribution of *Timon lepidus* on the Iberian Peninsula (Miraldo *et al.*, 2013). However, current *Timon* populations inhabit variable climatic zones around the Mediterranean, and some species seem to have speciated quite fast to adapt to new environmental conditions and ecological niches (Ahmadzadeh *et al.*, 2016). Therefore, it seems most plausible that the cause for extinction of large lizards on Sardinia was a combination of the evolution or introduction of new predators preying on small-sized animals (in particular *Cynotherium sardous*) and climatic changes.

CONCLUSIONS

Fossil remains of large-sized lacertid lizards from the late Pleistocene fissure fillings of Monte Tuttavista, Orosei (Sardinia, Italy), are described in detail herein, and trait variability is discussed. Cladistic analysis of an extensive, osteological phylogenetic matrix with 29 extant

and three extinct lacertid species, and three extant non-lacertid lizards as outgroups, recovers these remains as the sister taxon to the extant species of the genus *Timon*, so that we herein refer the material to *Timon* sp. This is the first report of this genus from Sardinia. Due to a high amount of homoplasy, and the finding of contradictory groups compared to established molecular phylogenies during a first unconstrained analysis, we had to implement a series of monophyly constraints for a second iteration of the phylogenetic analysis, where the extinct species were treated as wild-card taxa. Inclusion of the occurrences of *Timon* sp. in a biostratigraphic framework of the Sardinian mammal fauna shows that the disappearance of this large-sized lacertid broadly coincides with the appearance of the endemic canid *Cynotherium sardous*, which likely descended from a larger *Cynotherium* species that migrated to Sardinia in the early Pleistocene, and became adapted to catch smaller prey. The appearance of new, specialized predators, together with the severe climatic fluctuations during the Pleistocene, could therefore have played a role in the local extinction of *Timon* sp. and potentially other large reptiles on Sardinia.

ACKNOWLEDGMENTS

The compilation of the phylogenetic matrix would not have been possible without the logistic help of numerous people in collections visited between 2015 and 2017. These include Sónia Gabriel and Simon Davis (CIPA), Marta Calvo and Alberto Sanchez (MNCN), Jean-Claude Rage, Salvador Bailon and Virginie Bouetel (MNHN), Jeff Streicher and Patrick Campbell (NHMUK), Heinz Grillitsch, Georg Gassner and Silke Schweiger (NHMW), Christian Klug and Winand Brinkmann (PIMUZ), and Ralf Kosma (SRK). Additional specimens could be studied thanks to loans from HUIJ-OST, MRAC, UAM and ZZSiD. We would like to specifically thank Rebecca Biton, Georgios Georgalis and Mauro Grano, who personally brought specimens from these collections to Turin for us to study, and Annelise Folie, Francisco Ortega and Zbigniew Szyndlar for approving and organizing loans. We furthermore thank the Willi Hennig Society and the Mesquite Project Team for providing their software TNT and MESQUITE, respectively, for free online. Two anonymous referees provided numerous helpful comments on an earlier version of the manuscript, which greatly improved the quality of the paper.

FUNDING

The study was supported by the European Union's Seventh Framework programme for research and

innovation under the Marie Skłodowska–Curie grant agreement No. 609402-2020 researchers: Train to Move (T2M) (to E. Tschopp), and by several SYNTHESYS Projects (<http://www.synthesys.info/>), financed by the European Community Research Infrastructure Action under the FP7 ‘Capacities’ Programme. The collection visits funded through SYNTHESYS were at the MNHN (FR-TAF-5007 and 5839, to A. Villa and E. Tschopp, respectively) and the NHMW (AT-TAF-4591 and 5725, to A. Villa and E. Tschopp, respectively). M. Delfino is supported by the Fondi di Ateneo dell’Università di Torino (2015–16), Generalitat de Catalunya/CERCA Programme and the Agencia Estatal de Investigación (AEI) from Spain/European Regional Development Fund of the European Union (CGL2016-76431-P). E. Tschopp is currently supported through a Theodore Roosevelt Memorial Fund and Division of Paleontology Postdoctoral Research Fellowship from the Richard Gilder Graduate School at the American Museum of Natural History, New York, USA.

REFERENCES

- Abbazzi L, Angelone C, Arca M, Barisone G, Bedetti C, Delfino M, Kotsakis T, Marcolini F, Palombo MR, Pavia M, Piras P, Rook L, Torre D, Tuveri C, Valli AMF, Wilkens B. 2004.** Plio-Pleistocene fossil vertebrates of Monte Tuttavista (Orosei, Eastern Sardinia, Italy), an overview. *Rivista Italiana di Paleontologia e Stratigrafia* **110**: 681–706.
- Abbazzi L, Arca M, Tuveri C, Rook L. 2005.** The endemic canid *Cynotherium* (Mammalia, Carnivora) from the Pleistocene deposits of Monte Tuttavista (Nuoro, eastern Sardinia). *Rivista Italiana di Paleontologia e Stratigrafia (Research in Paleontology and Stratigraphy)* **111**: 497–511.
- Ahmadzadeh F, Carretero MA, Harris DJ, Perera A, Böhme W. 2012.** A molecular phylogeny of the eastern group of ocellated lizard genus *Timon* (Sauria: Lacertidae) based on mitochondrial and nuclear DNA sequences. *Amphibia–Reptilia* **33**: 1–10.
- Ahmadzadeh F, Flecks M, Carretero MA, Böhme W, Ihlow F, Kapli P, Miraldo A, Rödder D. 2016.** Separate histories in both sides of the Mediterranean: phylogeny and niche evolution of ocellated lizards. *Journal of Biogeography* **43**: 1242–1253.
- Al-Hassawi AMA. 2004.** *The osteology and myology of the cranio-cervical region in squamate reptiles: a comparative study.* Unpublished Ph.D. Thesis, University of London.
- Arnold EN. 1989.** Towards a phylogeny and biogeography of the Lacertidae: relationships within an Old-World family of lizards derived from morphology. *Bulletin of the British Museum, Natural History. Zoology* **55**: 209–257.
- Arnold EN, Arribas O, Carranza S. 2007.** Systematics of the Palaearctic and Oriental lizard tribe Lacertini (Squamata: Lacertidae: Lacertinae), with descriptions of eight new genera. *Zootaxa* **1430**: 3–86.
- Augé ML, Hervet S. 2009.** Fossil lizards from the locality of Gannat (late Oligocene–early Miocene, France) and a revision of the genus *Pseudeumeces* (Squamata, Lacertidae). *Palaeobiodiversity and Palaeoenvironments* **89**: 191.
- Augé ML, Bailon S, Malfay JP. 2003.** Un nouveau genre de lacertidae (Reptilia, Lacertilia) dans les faluns miocènes de l’Anjou-Touraine (Maine-et-Loire, France). *Geodiversitas* **25**: 289–295.
- Bailon S. 2004.** *Fossil records of Lacertidae in Mediterranean islands: the state of the art. Proceedings of the Fourth International Symposium of the Lacertids of the Mediterranean Basin.* Maó, Illes Balears, Spain: Institut Menorquí d’Estudis Maó, 37–62.
- Bailon S, Boistel R, Bover P, Alcover JA. 2014.** *Maioricalacerta rafelinensis*, gen. et sp. nov. (Squamata, Lacertidae), from the Early Pliocene of Mallorca (Balearic Islands, Western Mediterranean Sea). *Journal of Vertebrate Paleontology* **34**: 318–326.
- Bañuls Cardona S, López-García JM, Blain HA, Canals Salomó A. 2012.** Climate and landscape during the Last Glacial Maximum in southwestern Iberia: the small-vertebrate association from the Sala de las Chimeneas, Maltravieso, Extremadura. *Comptes Rendus Palevol* **11**: 31–40.
- Barahona F. 1996.** Osteología craneal de lacértidos de la Península Ibérica e Islas Canarias: análisis sistemático filogenético. Unpublished Ph.D. thesis, Universidad Autónoma de Madrid.
- Barahona F, Barbadillo LJ. 1997.** Identification of some Iberian lacertids using skull characters. *Revista Española de Herpetología* **11**: 47–62.
- Barahona F, Barbadillo LJ. 1998.** Inter- and intraspecific variation in the post-natal skull of some lacertid lizards. *Journal of Zoology* **245**: 393–405.
- Barahona F, Evans SE, Mateo JA, García-Márquez M, López-Jurado LF. 2000.** Endemism, gigantism and extinction in island lizards: the genus *Gallotia* on the Canary Islands. *Journal of Zoology* **250**: 373–388.
- Benítez de Lugo Enrich L, Palomares Zumajo N, Álvarez García HJ, Barroso Bermejo R, Benito Sánchez M, Blain HA, Bueno Ramírez P, Balbín Behrmann R de, Fernández Martín S, López Sáez JA, Galindo-Pellicena MÁ, Garrido Martínez MA, Laplana Conesa C, Mata Trujillo E, Menchén Herreros G, Montero Ruiz I, Moraleda Sierra J, Morgado Rodríguez A, Odriozola CP, Polo Martín E, Ruiz-Alonso M, Sevilla García P, Schuhmacher TX, Salazar-García DC. 2015.** *Paleoecología y cultura material en el complejo tumular prehistórico del Castilejo del Bonete*, Terrinches, Ciudad Real. *Menga: revista de prehistoria de Andalucía* **6**: 113–140.
- Blanford WT. 1874.** Description of new Reptilia and Amphibia from Persia and Baluchistan. *Annals and Magazine of Natural History* **4**: 31–35.
- Bochaton C, Boistel R, Casagrande F, Grouard S, Bailon S. 2016.** A fossil *Diploglossus* (Squamata, Anguillidae) lizard from Basse-Terre and Grande-Terre Islands (Guadeloupe, French West Indies). *Scientific Reports* **6**: 28475.
- Böhme M, Ilg A. 2003.** fosFARbase. Available at: <http://www.wahre-staerke.com> (accessed March 2017).

- Böhme W, Zammit-Maempel G. 1982.** *Lacerta siculimeliten-sis* sp. n. (Sauria: Lacertidae), a giant lizard from the late Pleistocene of Malta. *Amphibia-Reptilia* **3**: 257–268.
- Boulenger GA. 1881.** On the lizards of the genera *Lacerta* and *Acanthodactylus*. *Proceedings of the Zoological Society of London* **49**: 739–747.
- Brazeau MD. 2011.** Problematic character coding methods in morphology and their effects. *Biological Journal of the Linnean Society* **104**: 489–498.
- Brunner G. 1957.** Die Breitenberghöhle bei Gössweinstein ob Franken. *Neues Jahrbuch für Geologie und Paläontologie Monatshefte*: 352–403.
- Buchholz KF. 1963.** Die Perleidechse der Sierra Nevada (Reptilia: Lacertidae). *Bonner Zoologische Beiträge* **14**: 151–156.
- Calvino F, Dieni I, Ferasin F, Piccoli G. 1972.** *Note illustrative della Carta Geologica D'Italia Scala 1:100.000*, F° 195 Orosei. Roma, Italy: Istituto Superiore per la Protezione e la Ricerca Ambientale.
- Carranza S, Arnold EN, Amat F. 2004.** DNA phylogeny of *Lacerta (Iberolacerta)* and other lacertine lizards (Reptilia: Lacertidae): did competition cause long-term mountain restriction? *Systematics and Biodiversity* **2**: 57–77.
- Carretero MA. 2008.** An integrated assessment of a group with complex systematics: the Iberomaghrebian lizard genus *Podarcis* (Squamata, Lacertidae). *Integrative Zoology* **3**: 247–266.
- Čerňanský A, Smith KT, Klembara J. 2014.** Variation in the position of the jugal medial ridge among lizards (reptilia: squamata): its functional and taxonomic significance. *Anatomical Record (Hoboken, N.J.: 2007)* **297**: 2262–2272.
- Čerňanský A, Augé ML, Rage JC. 2015.** A complete mandible of a new amphisbaenian reptile (Squamata, Amphisbaenia) from the late middle Eocene (Bartonian, Mp 16) of France. *Journal of Vertebrate Paleontology* **35**: e902379.
- Čerňanský A, Klembara J, Smith KT. 2016.** Fossil lizard from central Europe resolves the origin of large body size and herbivory in giant Canary Island lacertids. *Zoological Journal of the Linnean Society* **176**: 861–877.
- Daudin FM. 1802.** *Histoire naturelle, générale et particulière des reptiles*. Paris, France: Imprimerie de F. Dufart.
- Daza JD, Abdala V, Thomas R, Bauer AM. 2008.** Skull anatomy of the miniaturized gecko *Sphaerodactylus roosevelti* (Squamata: Gekkota). *Journal of Morphology* **269**: 1340–1364.
- Delfino M. 2001.** Early Pleistocene *Lacerta* remains from Southern Italy (Apricena, Foggia). Is it *Lacerta siculimeliten-sis*? In: Vicente E, Crespo EG, eds. *Mediterranean basin lacertid lizards – a biological approach*. Lisboa, Portugal: Instituto da Conservação da Natureza, 21–26.
- Delfino M, Bailon S. 2000.** Early Pleistocene herpetofauna from Cava Dell'Erba and Cava Pirro (Apulia, Southern Italy). *Herpetological Journal* **10**: 95–110.
- Delfino M, Kotsakis T, Arca M, Tuveri C, Pitruzzella G, Rook L. 2008.** Agamid lizards from the Plio-Pleistocene of Sardinia (Italy) and an overview of the European fossil record of the family. *Geodiversitas* **30**: 641–655.
- Delfino M, Bailon S, Pitruzzella G. 2011.** The late Pliocene amphibians and reptiles from 'Capo Mannu D1 Local Fauna' (Mandriola, Sardinia, Italy). *Geodiversitas* **33**: 357–382.
- Depéret C. 1890.** *Les animaux pliocènes du Roussillon*. Paris, France: Librairie Polytechnique Baudry et cie.
- Díaz-Ruiz F, Delibes-Mateos M, García-Moreno JL, María López-Martín J, Ferreira C, Ferreras P. 2013.** Biogeographical patterns in the diet of an opportunistic predator: the red fox *Vulpes vulpes* in the Iberian Peninsula. *Mammal Review* **43**: 59–70.
- Dieni I, Massari F. 1966.** Il Neogene e il Quaternario dei dintorni di Orosei (Sardegna). *Memorie della Società Italiana di Scienze Naturali* **15**: 89–142.
- Dieni I, Massari F, Montanari L. 1966.** Il Paleogene dei dintorni di Orosei (Sardegna). *Memorie della Società Italiana di Scienze Naturali* **14**: 137–183.
- Estes R. 1983.** Handbuch der Paläoherpetologie. *Encyclopedia of Paleoherpetology. T. 10A. Sauria terrestria, Amphisbaenia*. Stuttgart, Portland-USA: G. Fischer.
- Estes R, Williams EE. 1984.** Ontogenetic variation in the molariform teeth of lizards. *Journal of Vertebrate Paleontology* **4**: 96–107.
- Estes R, De Queiroz K, Gauthier J. 1988.** Phylogenetic relationships within Squamata. In: Estes R, Pregill G, eds. *Phylogenetic relationships of the lizard families*. Palo Alto, USA: Stanford University Press, 119–281.
- Etheridge R. 1967.** Lizard caudal vertebrae. *Copeia* **1967**: 699–721.
- Evans SE. 2008.** The skull of lizards and tuatara. In: *Biology of the Reptilia*. Ithaca: SSAR, 1–347.
- Fernández Eraso J, García Rojas M, Fernández Crespo T, Castaños Ugarte PM, Bailon S, Murélagu Bereicua J, Tarrío Vinagre A. 2010.** La cueva de Las Orcillas 1: una estación de los últimos cazadores-recolectores en La Berrueza (Mendoza-Acedo, Navarra). *Trabajos de Arqueología Navarra* **22**: 13–91.
- Fu J. 1998.** Toward the phylogeny of the family Lacertidae: implications from mitochondrial DNA 12S and 16S gene sequences (Reptilia: Squamata). *Molecular Phylogenetics and Evolution* **9**: 118–130.
- Fu J. 2000.** Toward the phylogeny of the family Lacertidae – why 4708 base pairs of mtDNA sequences cannot draw the picture. *Biological Journal of the Linnean Society* **71**: 203–217.
- Fu J, Murphy RW, Darevsky IS. 1997.** Toward the phylogeny of Caucasian rock lizards: implications from mitochondrial DNA gene sequences (Reptilia: Lacertidae). *Zoological Journal of the Linnean Society* **120**: 463–477.
- Gauthier JA, Kearney M, Maisano JA, Rieppel O, Behlke ADB. 2012.** Assembling the squamate tree of life: perspectives from the phenotype and the fossil record. *Bulletin of the Peabody Museum of Natural History* **53**: 3–308.
- Georgalis GL, Zoboli D, Pillola GL, Delfino M. 2017.** A revision of the trionychid turtle *Procyclus sardus* Portis, 1901 from the late Miocene of Sardinia (Italy). *Annales de Paléontologie* **103**: 127–134.
- Goloboff PA, Farris JS, Nixon KC. 2008.** TNT, a free program for phylogenetic analysis. *Cladistics* **24**: 774–786.

- Harris DJ, Arnold EN, Thomas RH. 1998.** Relationships of lacertid lizards (Reptilia: Lacertidae) estimated from mitochondrial DNA sequences and morphology. *Proceedings of the Royal Society of London. Series B: Biological Sciences* **265**: 1939–1948.
- Harris DJ, Carretero MA. 2003.** Comments on the taxonomic value of (sub) genera within the family Lacertidae (Reptilia). *Amphibia–Reptilia* **24**: 119–122.
- Hoffstetter R. 1944.** Sur les Scincidae fossiles. I. Formes européennes et nord-américaines. *Bulletin du Muséum National d'Histoire Naturelle* **16**: 547–553.
- Hoffstetter R, Gasc JP. 1969.** Vertebrae and ribs of modern reptiles. In: Gans C, Bellairs A d'A, Parsons TS, eds. *Biology of the Reptilia*. London, UK: Academic Press, 201–310.
- Holman JA. 1998.** *Pleistocene amphibians and reptiles in Britain and Europe*. Oxford, UK: Oxford University Press.
- Kapli P, Poulakakis N, Lymberakis P, Mylonas M. 2011.** A re-analysis of the molecular phylogeny of Lacertidae with currently available data. *Basic and Applied Herpetology* **25**: 97–104.
- Klembara J, Böhme M, Rummel M. 2010.** Revision of the anguine lizard *Pseudopus laurillardii* (Squamata, Anguillidae) from the Miocene of Europe, with comments on paleoecology. *Journal of Paleontology* **84**: 159–196.
- Kotsakis T. 1977.** I resti di anfibi e rettili pleistocenici della grotta di Spinagallo (Siracusa, Sicilia). *Geologica Rom* **16**: 211–229.
- Kotsakis T, Delfino M, Piras P. 2004.** Italian Cenozoic crocodylians: taxa, timing and palaeobiogeographic implications. *Palaeogeography, Palaeoclimatology, Palaeoecology* **210**: 67–87.
- Lataste F. 1880.** Diagnose des reptiles nouveaux d'Algérie. 3. *Lacerta ocellata pater* (n. ssp.). *Le Naturaliste* **1880**: 306–307.
- Lécure S. 1968.** Remarques sur le scapulo-coracoïde des lacertiliens. *Annales des Sciences Naturelles, Zoologie, Paris* **10**: 475–510.
- Lécure S. 1969.** Étude morphologique de l'humérus des lacertiliens. *Annales des Sciences Naturelles, Zoologie, Paris* **11**: 515–558.
- Leppard TP. 2014.** Modeling the impacts of Mediterranean island colonization by archaic Hominins: the likelihood of an insular Lower Palaeolithic. *Journal of Mediterranean Archaeology* **27**: 231–253.
- Lyras G, van der Geer A. 2006.** Adaptations of the Pleistocene island canid *Cynotherium sardous* (Sardinia, Italy) for hunting small prey. *Cranium* **23**: 51–60.
- Lyras GA, van der Geer AAE, Rook L. 2010.** Body size of insular carnivores: evidence from the fossil record. *Journal of Biogeography* **37**: 1007–1021.
- Maddison WP, Maddison DR. 2017.** *Mesquite: a modular system for evolutionary analysis*. Available at <http://mesquiteproject.org> (last accessed February 2018)
- Marzahn E, Mayer W, Joger U, Ilgaz Ç, Jablonski D, Kindler C, Kumlutaş Y, Nistri A, Schneeweiss N, Vamberger M, Žagar A, Fritz U. 2016.** Phylogeography of the *Lacerta viridis* complex: mitochondrial and nuclear markers provide taxonomic insights. *Journal of Zoological Systematics and Evolutionary Research* **54**: 85–105.
- Masini F, Petruso D, Bonfiglio L, Mangano G. 2008.** Origination and extinction patterns of mammals in three central Western Mediterranean islands from the Late Miocene to Quaternary. *Quaternary International* **182**: 63–79.
- Mateo JA. 1988.** *Estudio sistemático y zoogeográfico de los lagartos ocellados*. Unpublished Ph.D. Thesis, University of Sevilla, Spain.
- Mateo JA. 2009.** Lagarto ocellado. *Timon lepidus* (Daudin, 1802). In: Salvador A, Marco A, eds. *Enciclopedia virtual de los vertebrados Españoles*. Madrid, Spain: Museo Nacional de Ciencias Naturales, 1–58.
- Mateo JA, López-Jurado LF. 1997.** Dental ontogeny in *Lacerta lepida* (Sauria, Lacertidae) and its relationship to diet. *Copeia* **1997**: 461–463.
- Mayer W, Bischoff W. 1996.** Beiträge zur taxonomischen revision der Gattung *Lacerta* (Reptilia: Lacertidae), Teil 1: *Zootoca*, *Omanosaura*, *Timon* und *Teira* als eigenständige Gattungen. *Salamandra* **32**: 163–170.
- Mendes J, Harris DJ, Carranza S, Salvi D. 2016.** Evaluating the phylogenetic signal limit from mitogenomes, slow evolving nuclear genes, and the concatenation approach. New insights into the Lacertini radiation using fast evolving nuclear genes and species trees. *Molecular Phylogenetics and Evolution* **100**: 254–267.
- Miraldo A, Faria C, Hewitt GM, Paulo OS, Emerson BC. 2013.** Genetic analysis of a contact zone between two lineages of the ocellated lizard (*Lacerta lepida* Daudin 1802) in south-eastern Iberia reveal a steep and narrow hybrid zone. *Journal of Zoological Systematics and Evolutionary Research* **51**: 45–54.
- Mlynarski M. 1956.** Lizards from the Pliocene of Poland. *Acta Palaeontologica Polonica* **1**: 135–152.
- Palombo MR. 2006.** Biochronology of the Plio-Pleistocene terrestrial mammals of Sardinia: the state of the art. *Hellenic Journal of Geosciences* **41**: 47–66.
- Palombo MR. 2009.** Biochronology, paleobiogeography and faunal turnover in western Mediterranean Cenozoic mammals. *Integrative Zoology* **4**: 367–386.
- Palombo MR, Rozzi R. 2014.** How correct is any chronological ordering of the Quaternary Sardinian mammalian assemblages? *Quaternary International* **328–329**: 136–155.
- Palombo MR, Antonioli F, Lo Presti V, Mannino MA, Melis RT, Orru P, Stocchi P, Talamo S, Quarta G, Calcagnile L, Deiana G, Altamura S. 2017.** The late Pleistocene to Holocene palaeogeographic evolution of the Porto Conte area: clues for a better understanding of human colonization of Sardinia and faunal dynamics during the last 30 ka. *Quaternary International* **439**: 117–140.
- Pregill G. 1984.** Durophagous feeding adaptations in an amphisbaenid. *Journal of Herpetology* **18**: 186–191.
- Pyron RA, Burbrink FT, Wiens JJ. 2013.** A phylogeny and revised classification of Squamata, including 4161 species of lizards and snakes. *BMC Evolutionary Biology* **13**: 93.
- Rauscher KL. 1992.** Die Echsen (Lacertilia, Reptilia) aus dem Plio-Pleistozän von Bad Deutsch-Altenburg, Niederösterreich. *Beiträge zur Paläontologie von Österreich* **17**: 81–177.

- Reeder TW, Townsend TM, Mulcahy DG, Noonan BP, Wood PL Jr, Sites JW Jr, Wiens JJ. 2015.** Integrated analyses resolve conflicts over squamate reptile phylogeny and reveal unexpected placements for fossil taxa. *PLoS ONE* **10**: e0118199.
- Roček Z. 1980.** Intraspecific and ontogenetic variation of the dentition in the green lizard *Lacerta viridis* (Reptilia, Squamata). *Vestník Československé Společnosti Zoologické* **44**: 272–278.
- Rook L, Ferretti MP, Arca M, Tiveri C. 2004.** *Chasmaporthetes melei* n.sp., an endemic hyaenid (Carnivora, Mammalia) from the Monte Tuttavista fissure fillings (Late Pliocene to Early Pleistocene; Sardinia, Italy). *Rivista Italiana di Paleontologia e Stratigrafia (Research In Paleontology and Stratigraphy)* **110**: 707–714.
- Russell AP, Bauer AM. 2008.** The appendicular locomotor apparatus of *Sphenodon* and normal-limbed squamates. In: Gans C, Gaunt AS, Adler K, eds. *Biology of the Reptilia. Volume 21. Morphology I. The skull and appendicular locomotor apparatus of Lepidosauria*. Ithaca, USA: Society for the Study of Amphibians and Reptiles, 1–465.
- Sagonas K, Poulakakis N, Lymberakis P, Parmakelis A, Pafilis P, Valakos ED. 2014.** Molecular systematics and historical biogeography of the green lizards (*Lacerta*) in Greece: insights from mitochondrial and nuclear DNA. *Molecular Phylogenetics and Evolution* **76**: 144–154.
- Schmidtler JF. 2010.** The taxonomic history of the Linnean genus *Lacerta* (Squamata: Sauria: Lacertidae) in the mirror of book-illustration. *Bonn Zoological Bulletin* **57**: 307–328.
- Sondaar PY, Sanges M, Kotsakis T, de Boer PL. 1986.** The Pleistocene deer hunter of Sardinia. *Geobios* **19**: 17–31.
- Suchov GF. 1936.** Eine neue Unterart der Eidechse aus dem persischen Kurdistan. *Travaux de l'Institut Zoologique de l'Académie des Sciences URSS* **3**: 303–308.
- Tschopp E. 2016.** Nomenclature of vertebral laminae in lizards, with comments on ontogenetic and serial variation in Lacertini (Squamata, Lacertidae). *PLoS ONE* **11**: e0149445.
- Tschudi JJ. 1836.** Über ein neues Subgenus von *Lacerta* Cuv. *Isis von Oken* **7**: 546–551.
- Vigne JD. 2014.** The origins of mammals on the Mediterranean islands as an indicator of early voyaging. *Eurasian Prehistory* **10**: 45–56.
- Villa A, Tschopp E, Georgalis GL, Delfino M. 2017.** Osteology, fossil record and palaeodiversity of the European lizards. *Amphibia-Reptilia* **38**: 79–88.
- Wiens JJ. 1995.** Polymorphic characters in phylogenetic systematics. *Systematic Biology* **44**: 482–500.
- Wiens JJ. 1998.** Testing phylogenetic methods with tree congruence: phylogenetic analysis of polymorphic morphological characters in phrynosomatid lizards. *Systematic Biology* **47**: 427–444.
- Wiens JJ. 2000.** Coding morphological variation within species and higher taxa for phylogenetic analysis. In: Wiens JJ, ed. *Phylogenetic analysis of morphological data*. Washington, DC, USA: Smithsonian Institution Press, 115–145.
- Willemsen GF. 1992.** A revision of the Pliocene and Quaternary Lutrinae from Europe. *Scripta Geologica* **101**: 1–115.

SUPPORTING INFORMATION

Additional Supporting Information may be found in the online version of this article at the publisher's web-site:

Table S1. Specimens studied from Monte Tuttavista, Orosei (Sardinia, Italy)

Table S2. Specimens studied first-hand, and literature resources for phylogenetic analysis

Matrix M1. Phylogenetic matrix (TNT input file)

Matrix M2. Phylogenetic matrix (MESQUITE file)

Table S3. List of apomorphies recovered for species and clades

Table S4. Measurements and quantitative character scores of the elements from Monte Tuttavista